Nature Communications

https://doi.org/10.1038/s41467-026-68966-4

Article in Press

FANCD2 restrains fork progression and prevents fragility at early origins upon re-replication

Received: 6 February 2025

Accepted: 21 January 2026

Cite this article as: Badra-Fajardo, N., Karydi, E., Bayona-Feliu, A. *et al.* FANCD2 restrains fork progression and prevents fragility at early origins upon re-replication. *Nat Commun* (2026). https://doi.org/10.1038/s41467-026-68966-4

Nibal Badra-Fajardo, Elena Karydi, Aleix Bayona-Feliu, Belén Gómez-González, Ourania Preza, Marina Arbi, Argyro Kalogeropoulou, Juha K. Rantala, Stavros Taraviras, Andrés Aguilera & Zoi Lygerou

FANCD2 restrains fork progression and prevents fragility at early origins upon re-replication

Nibal Badra-Fajardo[1], Elena Karydi[1], Aleix Bayona-Feliu[2], Belén Gómez-González[3], Ourania Preza[1], Marina Arbi[1], Argyro Kalogeropoulou[4], Juha K. Rantala[5], Stavros Taraviras[4], Andrés Aguilera[3] and Zoi Lygerou[1,*]

[1]Department of General Biology, Medical School, University of Patras, 26504 Patras, Greece
[2]Department of Genetics, Microbiology and Statistics, Faculty of Biology, Universitat de Barcelona, 08028 Barcelona, Spain
[3]Andalusian Center of Molecular Biology and Regenerative Medicine (CABIMER), Universidad de Sevilla, 41092 Seville, Spain
[4] Department of Physiology, Medical School, University of Patras, 26504 Patras, Greece
[5] Misvik Biology Oy, 20520 Turku, Finland

*Corresponding author: lygerou@upatras.gr

ABSTRACT

DNA replication is tightly regulated to ensure a single round of chromosome duplication per cell division. DNA licensing restricts origin firing to once-per-cell-cycle while aberrant licensing promotes re-replication and genome instability. Here, we investigate the mechanisms that protect genome integrity following re-replication induced by depletion of the licensing inhibitor Geminin. We find that re-replicating cells require FANCD2 to prevent genome instability. FANCD2 is rapidly recruited to chromatin upon Geminin loss, where it limits unrestrained fork progression and prevents single strand DNA gap accumulation and fork breakage. Genome-wide analyses reveal that upon re-replication, FANCD2 localizes to early origins within highly transcribed regions prone to accumulate R-loops and enriched in early replicating fragile sites. Importantly, reducing transcription and R-loops alleviates re-replication-induced genome fragility whereas PARP inhibition exacerbates it. Our study uncovers a role for FANCD2 in safeguarding genome integrity during re-replication, offering avenues for selective targeting of cancer cells.

Introduction

Accurate DNA duplication is essential during somatic cell division to ensure the inheritance of a complete copy of parental DNA by the offspring. In eukaryotes, replication initiates from discrete genomic regions known as origins, which are spatially distributed along the chromosome and become activated in clusters that follow a defined temporal program to achieve the complete replication of the genome[1,2]. Replication initiation is mediated by two major steps that are temporarily spaced by the different activity of cyclin-dependent kinases: origin licensing (helicase loading) in G1 and origin firing (helicase activation) in S-phase. Origin licensing refers to the assembly of pre-replicative complexes (pre-RCs) containing the origin recognition complex (ORC), CDC6 and CDT1, and the inactive form of the mini-chromosome maintenance 2-7 (MCM) helicase onto each origin of replication[3-7], whereas origin firing entails the recruitment of additional replication factors for the conversion of pre-RCs into active replisomes[8-10]. Uncoupling between licensing and firing is crucial to ensure that no genomic region is left un-replicated while limiting single origin firing to once per cell cycle[11,12]. Among all the licensing proteins involved in pre-RC formation, CDT1 undergoes the greatest control mechanisms as it recruits soluble replicative helicases from the nucleus to ORC and CDC6-bound origins[13,14]. Consistently, earlier work showed that aberrant CDT1 activity induces re-replication and DNA breakage across species. Over-expression of CDT1 in fission yeast cells leads to re-replication and gene amplification[15]. Accordingly, addition of CDT1 to *X. laevis* eggs or over-expression of the ortholog of CDT1 in *Drosophila* is sufficient to induce re-replication and DNA damage[16,17]. In mammalians, ectopic expression of CDT1 promotes re-replication and tumorigenesis[18-22], and inhibition of its ubiquitin-mediated proteolysis has demonstrated to induce apoptosis in several cancer models[23,24].

Besides transcriptional control of CDT1 expression and fine-tuning over its activity through the ubiquitin proteasome system[25], timely regulation of CDT1 depends on Geminin, a small protein only present in metazoans that acts as an inhibitor of pre-RC assembly by direct binding to CDT1 in S and G2[26-29]. Control over DNA licensing by Geminin is considered a redundant mechanism in metazoa to prevent any non-degraded and nuclear-free CDT1 from initiating illegitimate licensing of origins outside of G1. According to this, Geminin loss induces re-replication and DNA damage selectively in cancer cells[30,31], which usually exhibit an abnormal expression of several licensing factors and compromised tumor barriers[32]. These results are consistent with analysis *in vivo*, where Geminin ablation has demonstrated to favor tumorigenesis and induces cell death in neural stem cells during development[33,34]. The dependency of highly proliferative cells on Geminin could be a genomic trait of therapeutic significance in cancer, and small molecules phenocopying the effects of inhibiting Geminin activity are being currently

characterized with promising results[35,36]. The increasing evidence suggesting that re-replication is a driving force of tumorigenesis argues for a better understanding of the mechanisms detecting and preventing re-replication associated DNA lesions.

Here, we show that cells depleted of Geminin require FANCD2 to promote cell survival and prevent deleterious levels of DNA damage. FANCD2 is pivotal during repair of inter-strand crosslinks (ICLs)[37], but recent studies have demonstrated that it also plays a fundamental role during replication stress by promoting fork stability[37]. Our results indicate that Geminin depletion induces FANCD2 recruitment onto chromatin early during the first round of replication, which is required to limit the unrestrained progression of re-replicating forks. Consequently, loss of FANCD2 in Geminin-deficient cells triggers the accumulation of single strand DNA (ssDNA) gaps and leads to massive fork breakage, which ultimately results in increased genomic instability. Genome-wide analysis of FANCD2 distribution on chromatin upon Geminin depletion demonstrates its enrichment at early DNA origins localized within highly transcribed genes, which are characterized by increased levels of transcription-replication conflicts (TRCs) and DNA damage. The results in this study reveal a function of FANCD2 in the maintenance of genome stability upon re-replication and provide insights into the clinical potential of targeting Geminin in FA/BRCA-deficient cancers.

Results

High-content screening identifies FANCD2 as essential to prevent DNA damage in Geminin-depleted cells

To identify mechanisms involved in the detection and repair of DNA lesions associated with aberrant licensing, we examined the effects of Geminin depletion on re-replication and DNA damage across different cell lines. We performed flow cytometry on Geminin-depleted and EdU pulse-labeled cells at different time points, which allowed us to measure the prevalence of cells with a DNA content greater than G2/M that were incorporating EdU as a metric for re-replication. As an alternative approach to quantify the levels of re-replication, we also measured nuclear areas[39], while we analyzed γH2AX and 53BP1 signals as proxies of DNA double-strand breaks (DSBs). Depletion of Geminin in U2OS cancer cells resulted in an initial accumulation of cells in S phase within the first 24 hours, with a small proportion undergoing re-replication (>4C DNA content) (Supplementary Figure 1a). A high prevalence of re-replicating cells was observed by 48hs, at which point approximately 30% of cells showed >4C DNA content and active EdU incorporation (Supplementary Figure 1a). These results were also reproduced by measuring nuclear areas (Supplementary Figure 1b) and were also accompanied by a significant increase

in γH2AX and 53BP1 signals (Supplementary Figure 1c). Co-depletion of CDT1 partially suppressed these phenotypes (Supplementary Figure 1d), indicating that these effects are dependent on active DNA replication. In contrast, depletion of Geminin in non-cancerous hTERT-RPE1 cells had minimal effects on re-replication and DNA damage (Supplementary Figure 1e-g), supporting the notion that Geminin prevents re-replication selectively in cancer cells[30,31]. Accordingly, Geminin depletion increased DNA damage in MCF7 cancer cells but had a minor effect in the non-tumorigenic MCF10A cell line (Supplementary Figure 1h).

The mild effects observed in hTERT-RPE1 cells 48hs after Geminin depletion provided an ideal system to achieve low-level re-replication and prompted us to employ this cell line to perform a high-content screening for factors required to maintain genome stability in cells primed for re-replication. To that end, we used a custom-designed siRNA library targeting 300 genes associated with the DNA damage response (DDR) and DNA repair pathways (Supplementary Data 1). After transient transfection with the siRNA library, control and Geminin-depleted hTERT-RPE1 cells were pulse-labelled with EdU for 1 hour prior to fixation, and total cell counts, as well as EdU and γH2AX signal intensities were measured as markers of cell viability and DNA damage (Fig. 1a).

The results of the screen yielded two distinct classes of candidates, consisting of genes whose depletion was toxic to both cell lines (Geminin-depleted and control), which served as a control to validate the methodology of the screening, and a second class, comprising genes whose depletion was particularly toxic to Geminin-depleted cells, which were identified as hits. As expected, among the top-scoring genes whose downregulation increased DNA damage and compromised survival of both Geminin-depleted and control cells, we identified critical regulators of the cell cycle and cell cycle-checkpoint pathways[40-42] (i.e. PLK1, WEE1 or CHK1) (Fig. 1b and Supplementary Data 2). Concentrating on the candidates whose downregulation increased DNA damage or interfered with survival specifically in Geminin-depleted cells, we identified BRWD3, a histone reader and substrate of the Cullin4-DDB1 E3 ubiquitin ligase complex[43], and the pro-survival and BCL2-related protein BCL2L2[44] as top hits (Fig. 1b and Supplementary Data 2). Importantly, among the top candidates increasing DNA damage specifically in Geminin-depleted cells, we also found FANCD2 (Fig. 1b and Supplementary Data 2), a central component of the FA pathway traditionally associated with repair of ICLs[37]. Interestingly, other FA signaling components which cooperate with FANCD2 during ICL repair (such as BRCA1/2 or ERCC1) did not score positive in our screening (Supplementary Data 2), suggesting that the role of FANCD2 during re-replication is independent from its canonical ICL repair function. These results, together with the growing evidence supporting a critical role for FANCD2 in maintaining replication fork

stability[38], led us to prioritize this candidate for further analyses. Thus, we validated our results from the screening with a different set of siRNAs, which confirmed increased γH2AX intensities and 53BP1 foci (Fig. 1c) and revealed a significant reduction in long-term cell survival, as measured by clonogenic assays (Fig. 1d), in double Geminin and FANCD2 knockdowns when compared to control or single-depleted cells.

A similar effect was observed in cancer cells with high levels of re-replication; Specifically, this was confirmed in U2OS cells in which Geminin was depleted by siRNA or through a doxycycline-inducible shRNA (Supplementary Figure 2a, b, and Supplementary Figure 3a, b), as well as in HCT116 cells containing an auxin-inducible degron (AID)[45] for total inactivation of Geminin (Supplementary Figure 3c). Of note, co-depletion of Geminin and FANCD2 impaired long-term clonogenic survival but did not induce early apoptotic cell death, as demonstrated by analysis of AnnexinV+-PI and cleaved Caspase-3 (Supplementary Figure 2c). These results are in line with the limited effects observed in cell counts during the screen (Fig. 1b and Supplementary Data 2) and exclude the possibility that the effects are due to acute cytotoxicity.

Additionally, these results were further supported by assessing the effect of Geminin depletion in FANCD2-KO PD20 cells derived from a FA-D2 patient. As expected, silencing of Geminin induced significant levels of DSBs and reduced cell viability in PD20 cells (Supplementary Figure 3d, e). Importantly, introduction of the corrected wild-type (WT) FANCD2 rescued these phenotypes to basal levels (Supplementary Figure 3d, e), altogether suggesting that Geminin-depleted cells require FANCD2 to limit extensive DNA damage and promote cell survival.

FANCD2 is recruited at re-replicating forks prior to massive DNA breakage

To explore the potential contribution of FANCD2 in preventing DSBs during re-replication, we initially examined its localization on chromatin. Subcellular fractionation of U2OS cells depleted of Geminin revealed increased FANCD2 recruitment to chromatin (Fig. 2a). Consistently, Geminin depletion also induced the formation of FANCD2 foci, which localized near γH2AX sites (Fig. 2b). To determine whether FANCD2 activation is a general response to re-replication, we also analyzed the formation of FANCD2 foci following mild overexpression of CDT1. Since transient overexpression of this protein induces massive re-replication in cancer cells[46], we generated a stable clone expressing a CDT1-GFP fusion integrated into the genome of hTERT-RPE1 cells. This clone exhibited cell cycle-regulated CDT1 expression at levels 2-3 times higher than endogenous CDT1, sufficient to induce DNA damage without massively altering re-replication, as demonstrated by analysis of γH2AX intensities and nuclear areas (Supplementary Figure 4a, b).

As expected, over-expression of CDT1 in hTERT-RPE1 cells led to an increase in the proportion of cells with FANCD2 foci when compared to GFP-NLS control cells (Supplementary Figure 4b), suggesting that FANCD2 is actively recruited to chromatin upon re-replication. Moreover, analysis of publicly available (TCGA) data (https://www.cbioportal.org) revealed an upregulation of FANCD2 in subgroups of bladder, uterine and breast cancers with high CDT1 expression (Supplementary Figure 4c), consistent with an association of FANCD2 with aberrant DNA licensing.

Given that FANCD2 recruitment on chromatin is considered a consequence of replication fork blockage[47-50], and our results in U2OS cells demonstrating an initial accumulation of cells in S prior to high levels of re-replication (Supplementary Figure 1a), we hypothesized that Geminin depletion could trigger FANCD2 recruitment at stalled forks prior to the formation of widespread DSBs. To test this hypothesis, we measured the presence of FANCD2 foci and the increase in γH2AX nuclear intensities in Geminin-depleted U2OS cells in a time-course experiment. FANCD2 foci were observed as early as 12 hours after siRNA transfection whereas γH2AX did not significantly accumulate until 48 hs (Fig. 2c). Consistent with the analysis of FANCD2 foci, we did not observe a significant increase in the nuclear area until 12 hs after transfection (Supplementary Figure 5a), suggesting that upon Geminin depletion, FANCD2 recruitment on chromatin occurs early upon re-replication and precedes DNA breakage.

To further explore the dynamics of FANCD2 recruitment during re-replication, we performed a synchronization experiment in Geminin-depleted U2OS cells. Cells were arrested at G2/M by a sequential block with thymidine and the CDK1 inhibitor RO-3306, depleted of Geminin and then released into the next cell cycle (Supplementary Figure 5b). To follow FANCD2 recruitment as cell progressed through S and G2 phases, cells were pulse-labelled with EdU and immunostained against FANCD2, together with the replication stress marker RPA32, and the G2/M marker pH3 (H3-Ser10Pho). While control cells showed the characteristic early, middle and late S-phase EdU patterns as cells progressed through S-phase, in Geminin-depleted cells a population with a particular diffused EdU pattern was evident from 14 hs post-release, termed “R” from re-replicating (Fig. 2d). This cell population, which was actively synthesizing DNA, increased progressively and accumulated at the G2/M boundary, as shown by EdU incorporation in pH3-positive cells (Supplementary Figure 5c). In parallel to the appearance of re-replicating cells, FANCD2 and RPA32 foci increased significantly in Geminin-depleted cells from 14 hs post-release and accumulated at later time-points (Fig. 2e). Importantly, FANCD2 and RPA32 foci accumulation was evident specifically in re-replicating cells, as judged by the EdU pattern, and persisted as cells accumulated at G2/M (Supplementary Figure 5c, d), indicating that re-

replication upon Geminin loss begins within the first round of DNA synthesis and leads to early FANCD2 recruitment and RPA32 accumulation.

Next, to investigate whether FANCD2 is actively recruited at the vicinity of re-replicating forks, we pulse-labelled Geminin-depleted cells with EdU and monitored FANCD2 interaction with the newly synthesized DNA by proximity ligation assays (PLA). Geminin depletion significantly increased the number of EdU-FANCD2 PLA foci when compared to control cells (Fig. 3a). These results were also reproduced when we quantified the number of interacting PLA foci between FANCD2 and other replisome factors such as MCM2 or PCNA (Fig. 3b and Supplementary Figure 5e). Notably, the interaction between the replisome and FANCD2 not only occurred in S-phase cells but became evident in those cells exhibiting the characteristic EdU incorporation pattern of re-replicating cells (Fig. 3b). Altogether, these results suggest that re-replication upon Geminin loss begins within the first round of DNA synthesis and induces FANCD2 recruitment to active forks prior to G2/M arrest and high levels of DNA damage.

FANCD2 limits fork progression in Geminin-depleted cells upon checkpoint activation

Given its accumulation at re-replicating forks, we next sought to determine whether FANCD2 was required to limit the extent of re-replication. Interestingly, co-depletion of Geminin and FANCD2 in U2OS cells did not increase the percentage of EdU positive cells with a DNA content >4C nor the nuclear size above that of Geminin-depleted cells, but on the contrary slightly reduced it (Fig. 3c, d). These results were also reproduced in hTERT-RPE1 cells (Supplementary Figure 6a), excluding the possibility that FANCD2 restricts re-replication upon Geminin-depletion.

To further explore the dynamics of replication in cells depleted of Geminin and FANCD2, we then analyzed the progression of forks by DNA fiber assays. Double Geminin and FANCD2-depleted cells significantly increased fiber tract length and fork asymmetry (Fig. 3e), suggesting that FANCD2 limits fork speed and prevents fork stalling in the absence of Geminin. Although we could not measure origin distances due to DNA fiber analysis limitations, we observed that Geminin-depleted cells showed a slight increase in origin firing (Fig. 3f), according to the idea that over-licensing can also lead to ectopic origin firing[32]. However, downregulation of FANCD2 did not significantly alter the percentage of origin initiation (Fig. 3f), arguing against a primarily role for this protein in preventing ectopic firing of origins in the context of re-replication. Additionally, we investigated the effect of co-depleting Geminin and FANCD2 on cell cycle progression, using EdU incorporation and pH3 as markers of S and G2/M phases, respectively. According to the results obtained during synchronization experiments, Geminin depletion led to an increased proportion of cells retaining active DNA synthesis in G2, while they also exhibited high levels of

DNA damage (Fig. 3g and Supplementary Figure 6b). Geminin-depleted cells also demonstrated increased levels of phosphorylated Chk1 (Fig. 3h), in agreement with re-replication triggering checkpoint activation[51-53]. Indeed, inhibition of the G2/M checkpoint by incubating Geminin-depleted cells with a low dose of the VE-821 ATR inhibitor or with the general checkpoint inhibitor caffeine suppressed re-replication and the associated DNA damage phenotypes (Supplementary Figure 6c, d). This suggests that overriding the G2/M checkpoint force Geminin-depleted cells into mitosis prematurely, leaving insufficient time for extensive re-replication to occur. Consistent with this, incubation of Geminin-depleted cells with VE-821 resulted in the accumulation of inherited DNA lesions, as shown by increased micronuclei, aberrant mitosis, and reduced cell survival (Supplementary Figure 6e, f). Importantly, co-depletion of Geminin and FANCD2 further increased the percentage of G2-arrested and EdU-positive cells, while it retained checkpoint activity (Fig. 3g, h), suggesting that FANCD2 is not required for checkpoint activation in response to re-replication. Collectively, these results indicate that depletion of FANCD2 accelerates fork speed and causes DNA damage upon checkpoint activation in Geminin-depleted cells.

Loss of FANCD2 promotes the accumulation of ssDNA gaps and genomic instability in Geminin-depleted cells

Unrestrained fork progression promotes the accumulation of ssDNA gaps[54,55]. These gaps may lead to excessive RPA loading and subsequent depletion of the available RPA pool, leading to fork breakage and genome instability[56-58]. To determine whether the abnormal progression of forks in double Geminin and FANCD2-depleted cells correlated with an accumulation of ssDNA gaps, we analyzed the formation of RPA foci. Depletion of Geminin and FANCD2 triggered the accumulation of RPA foci exclusively in re-replicating cells, as shown by colocalization of pre-extracted RPA32 and pH3 positive cells (Fig. 4a and Supplementary Figure 7a). Notably, the intensity of RPA foci was also significantly increased in double-depleted cells (Supplementary Figure 7b), likely due to longer ssDNA gaps. As an alternative way to visualize ssDNA, we also labeled the cells with the nucleotide analogue BrdU, which was then detected by immunofluorescence under native conditions. Consistent with the results observed during analysis of RPA32 foci, Geminin depletion induced the formation of BrdU foci while the proportion of cells exhibiting BrdU foci was further increased upon co-depletion with FANCD2 (Fig. 4b). To further confirm the presence of ssDNA gaps, we performed a DNA fiber assay in cells depleted of Geminin and FANCD2 and incubated with the S1 endonuclease. Labelled nascent DNA tracks were shorter and thus sensitive to the S1 enzyme in double Geminin and FANCD2-depleted cells compared to single-depleted and control cells (Fig. 4c). The shortening in tract lengths observed

upon incubation of Geminin and FANCD2-double depleted cells to S1 nuclease was similar to that observed in cells incubated with the PARP inhibitor Olaparib (Fig. 4d). This is consistent with previous findings showing that PARPi sensitivity correlates with fork acceleration and gap formation[58,59]. Indeed, cells depleted of Geminin slightly increased the levels of parylation (Fig. 4d) whereas PARP inhibition in Geminin-depleted cells induced sensitivity to S1 nuclease activity and accumulation of RPA32 and BrdU foci, together with increased DSBs and reduced cell viability (Fig. 4e and Supplementary Figure 7c-e). This reinforces the idea that an excess of ssDNA gaps underlies the high levels of genomic instability observed in re-replicating cells upon Geminin loss.

Finally, we tested whether increased formation of ssDNA gaps and accumulation of DNA damage in Geminin and FANCD2 double-depleted cells would result in chromosome breakage and high levels of genomic instability. As anticipated, metaphase spreads from Geminin-depleted cells already exhibited an increased number of chromosome breaks and aberrations (Fig. 4f). However, depletion of FANCD2 in Geminin-defective cells further exacerbated these phenotypes (Fig. 4f). Additional signatures of persistent genomic instability, such as 53BP1 nuclear bodies or micronuclei were also increased in Geminin and FANCD2 double-depletes across different cell lines (Fig. 4g and Supplementary Figure 7f, g). Altogether, the results suggest that FANCD2 prevents the accumulation of ssDNA gaps and deleterious levels of DNA damage upon Geminin loss.

Contribution of FANCD2 mono-ubiquitination to cell survival during re-replication

The role of FANCD2 during replisome surveillance occurs independently of its mono-ubiquitination by the FA core complex, while it is required to preserve fork stability upon acute replication stress[37,60]. To explore the requirement of FANCD2 mono-ubiquitination for its function in sustaining the survival of re-replicating cells, we depleted FANCA -a key subunit of the E3 ubiquitin-ligase FA core complex- in Geminin-depleted cells. Consistent with the results obtained during chromatin fractionation, depletion of Geminin induced mono-ubiquitination of FANCD2 (Fig. 5a), while depletion of FANCA reduced total FANCD2 levels (Fig. 5a), as previously described[54]. Our analyses also revealed increased DSBs (Fig. 5b) and accumulation of RPA foci (Fig. 5c) in double Geminin and FANCA-depleted cells in comparison to single Geminin-depleted cells. Moreover, clonogenic assays showed reduced survival of Geminin-deficient cells upon FANCA depletion (Fig. 5d), although this effect was less pronounced than that observed upon FANCD2 loss. Consistent with this partial effect, FANCD2 foci, although significantly reduced, could still be detected on chromatin in Geminin and FANCA double-depleted cells (Fig. 5e).

To further explore the contribution on FANCD2 mono-ubiquitination for survival of re-replicating cells, we evaluated the clonogenic capacity of FANCD2-KO U2OS cells reconstituted with either FANCD2-WT or the ubiquitination-resistant FANCD2-K561R mutant to Geminin depletion (Fig. 5f). As anticipated, depletion of Geminin in FANCD2-KO cells induced massive cell death (Fig. 5g) in respect to control cells. Interestingly, while introduction of FANCD2-WT significantly improved cell viability in Geminin-depleted cells, depletion of Geminin in cells expressing the FANCD2-K561R mutant showed an intermediate clonogenic outgrowth (Fig. 5g). These results are consistent with residual levels of chromatin-bound, non-ubiquitinated FANCD2 partially rescuing replication fork restart and cell proliferation upon replication stress[61-63]. Thus, our data indicate that FANCD2 mono-ubiquitination contributes to preserve cell survival upon re-replication and suggest an additional ubiquitination-independent role protecting genome integrity.

Geminin depletion triggers FANCD2 enrichment at early origins within highly transcribed genes

To identify hotspots of fork stalling upon re-replication, we investigated FANCD2 localization genome-wide by ChIP-seq analyses in Geminin-depleted K562 lymphoblast cells, isolated from the bone marrow of a patient with myelogenous leukemia and extensively employed for comprehensive genomic studies[63]. Of note, depletion of Geminin in K562 cells promoted a re-replication phenotype similar to that observed in U2OS, as demonstrated by increased nuclear area, formation of FANCD2 foci and DNA damage (Supplementary Figure 8a). FANCD2 ChIP-seq were performed in duplicates, revealing a high correlation between replicates (Supplementary Figure 8b). The analysis identified 910 peaks with high FANCD2 levels that were common between control and Geminin-depleted cells, although most of them (4637 peaks in control vs 4681 in Geminin-depleted cells) showed a lower coverage and were condition specific (Fig. 6a, b). FANCD2 was slightly enriched at common fragile sites (CFSs) in control cells with respect to Geminin-depleted cells (Fig. 6c), consistent with previous reports demonstrating FANCD2 localization at these regions even under unperturbed conditions[65,66]. However, FANCD2 seemed to relocate to replication origins[66] in Geminin-depleted cells (Fig. 6c), suggesting that replication forks stall close to replication origins upon Geminin loss.

Similarly, a substantial number of genes (1,428 in total) were enriched in FANCD2 in both control and Geminin-depleted cells, although most of them were condition-specific (2,040 genes in Geminin-depleted cells vs 1,843 in control cells) (Fig. 6d). Those genes specifically enriched in FANCD2 upon Geminin depletion exhibited a shorter average length but higher GC content and expression levels than those specifically enriched in control cells (Fig. 6d). Moreover, analysis of

the functional elements of such FANCD2-enriched genes in Geminin-depleted cells revealed a significant accumulation at promoters and 5'UTRs (Fig. 6e). Since replication has been shown to initiate at the vicinity of active transcription start sites[67], these results align with the observed accumulation of FANCD2 at origins (Fig. 6c), and support that replication forks stall close to origins upon Geminin loss. To further explore this possibility, we performed a comparative analysis of FANCD2-enriched genes in relation to their closest replication origins. As expected, only 127 origins were found in common to both conditions, while 4526 and 4808 were specific in control or Geminin-depleted cells (Supplementary Figure 8c). This indicates that there is a different subset of replication origins in each condition from which replication forks stall and lead to FANCD2 enrichment. Consistent with peak analysis (Fig. 6c, e), more than 90% of the origins specifically found enriched in FANCD2 upon Geminin depletion colocalized with genes (Supplementary Figure 8c), thus indicating these origins lie within genes. These origins also exhibited higher FANCD2 levels when compared to those found in the control (Supplementary Figure 8d), as well as increased GC content and active transcription marks, including H4K20me, H3K4me1 and H3K27ac, and high levels of RNAP II Ser5P[65-68] (Supplementary Figure 8e). Thus, Geminin depletion leads to FANCD2 enrichment at intragenic replication origins within highly transcribed genes genome wide.

FANCD2 limits R-loop-associated fragility in Geminin-depleted cells

Intragenic origins mapping within highly transcribed genes have been shown to fire early during S phase upon oncogene-induced replication stress[72]. Furthermore, early replicating regions have been associated with transcriptionally active sites and accessible chromatin configuration[70,71]. Thus, we wondered whether Geminin depletion leads to fork stalling during early replication. Based on the analysis of publicly available Repli-seq datasets from the ENCODE project, which map replication timing across individual S subphases at specific genomic sites[75], we observed a significant increase in BrdU intensity during early S phase, and a reduction in mid-to-late replication timing in those origins identified to accumulate FANCD2 specifically in Geminin-depleted cells when compared to control cells (Fig. 6f), suggesting these origins replicate early.

Transcriptional activity at early replicating regions has been linked to DNA damage and DNA-RNA hybrids at early replicating fragile sites (ERFSs)[73,74]. Thus, we analyzed the levels of DNA damage and DNA-RNA hybrids from available γH2AX ChIP-seq[78] and DRIPc-seq[79] data of wild-type K562 cells. γH2AX signal was higher in those genes specifically enriched in FANCD2 upon Geminin loss (Fig. 7a). In addition, and despite DNA-RNA hybrid distribution profiles were similar, these genes exhibited higher DRIPc-seq signal levels (Fig. 7b). These results suggest

FANCD2 accumulation upon Geminin depletion occurs at R-loop containing regions that are prone to break even under unperturbed conditions, suggesting they could correspond to ERFSs. By lifting over ERFS data from synchronized mouse B cells[76] employing the LiftOver (UCSC) alignment tool, we analyzed FANCD2 coverage over potential human ERFSs. Strikingly, metagenomic analyses showed a significant accumulation of FANCD2 at ERFSs in Geminin-depleted cells (Fig. 7c). Altogether, these results suggest that re-replication upon Geminin depletion leads to the expression of ERFSs, supporting a model in which active transcription and R-loops cause fork stalling close to early replicating regions, thus contributing to genome instability. To test this hypothesis, we used the adenosine analog Cordycepin and we over-expressed RNase H1 to examine the effect of inhibiting general transcription or degrading DNA-RNA hybrids in replication fork stalling (FANCD2 foci), ssDNA gaps (RPA foci) and DSBs (γH2AX foci) upon Geminin depletion. Cordycepin treatment effectively reduced EU incorporation (Supplementary Figure 8f), supporting its role as a general transcription inhibitor. However, we were able to observe that it also caused a reduction in EdU incorporation, which could partially impact S-phase progression. This was not the case for cells over-expressing RNase H1, where bulk EdU incorporation remained unaffected (Supplementary Figure 8g). Importantly, both treatment with Cordycepin and RNase H1 over-expression significantly reduced the number of γH2AX, FANCD2 and RPA foci of Geminin-depleted cells (Fig. 7d, e). These results support that aberrant origin licensing and re-replication upon Geminin loss promotes fragility of ERFSs, which is prevented by FANCD2 recruitment.

Discussion

Strict regulation of DNA licensing is pivotal to ensure complete genome duplication while restricting origin firing to once per cell cycle. Current data suggest that aberrant licensing triggers re-activation of already fired origins, leading to re-replication as a source of genome instability and tumorigenesis. Earlier studies have addressed the consequences of inducing massive re-replication in cells[20,53,55,77,78], but the mechanisms involved in regulating mild levels of re-replication and protecting the survival of cells presenting these type of aberrations are not yet fully understood. In this study, we performed a siRNA screening for suppressors of DNA damage in cells exhibiting mild levels of re-replication through depletion of Geminin and identified a previously uncharacterized role of FANCD2 in protecting re-replicating cells from deleterious levels of genomic instability. This function of FANCD2 partially depends on its mono-ubiquitination activity and is critical to suppress an excess of post-replicative ssDNA gaps. Upon inhibition of

FANCD2, unrestrained progression of replisomes results in TRCs and the generation of ssDNA gaps that are converted into DSBs through the advancement of re-replicating forks, an event that becomes more frequent as the proportion of re-replicating forks is increased (Fig. 7f).

Our model is supported by several observations; FANCD2 recruitment begins early after Geminin depletion, followed by the accumulation of G2/M-arrested cells actively incorporating EdU and exhibiting increased DNA damage (Fig. 2 and 3). Although DNA damage signaling could contribute to FANCD2 localization in G2, we demonstrate that FANCD2 accumulation occurs specifically at the vicinity of re-replicating forks (Fig. 3). Although origin firing is not altered, we observe evidence of unrestrained DNA synthesis in cells co-depleted of Geminin and FANCD2. Specifically, double-depleted cells show a significant increase in both replication tract length and the presence of single-stranded DNA (ssDNA) gaps when compared to single-depleted or control cells (Fig. 3 and 4). This was verified by analysis of RPA32 foci and BrdU foci under non-denaturing conditions, as well as DNA fiber assays both alone and combined with S1 nuclease treatment. We further show that cells with high levels of ssDNA gaps arrest at G2/M, where they concomitantly incorporate EdU and exhibit high levels of DNA damage (Fig. 3 and 4) altogether indicating that re-replication leads to unrestrained DNA synthesis and subsequent fork breakage[17]. In agreement, it is known that the extensive accumulation of RPA at newly generated ssDNA precedes fork collapse[56]. Moreover, incubation of Geminin-depleted cells in the presence of ATRi abrogates the G2/M checkpoint and re-replication-associated DNA damage marks, whereas PARP inhibition exacerbates genome fragility (Fig. 4 and Supplementary Figure 6 and 7). Finally, our results also reveal that upon re-replication, FANCD2 is critical to prevent transcription-associated DNA damage particularly at early replicating sites, as inhibition of transcription or removal of R-loops reduce replication stress and DNA damage in Geminin-depleted cells (Fig. 6 and 7), altogether suggesting that active transcription contributes to genomic instability upon re-firing of DNA origins.

Although re-replication is associated with gene amplification and copy number gains in cancer[82], the mechanism underlying the expansion of gene copy numbers remains unclear. Our work supports that re-replication induces fork breakage after encountering ssDNA gaps that are in close proximity to the origins of replication. This might explain the low processivity of re-replicating forks and the configuration of repeat gene expansion flanking re-activated origins that is observed in different organisms[77,80]. These results predict that the genotoxic effects resulting from re-replication should correlate with the magnitude of discontinuities created on the template. Indeed, Geminin and FANCD2 double-depleted cells show increased fork speed, high levels of ssDNA gaps and DNA damage (Fig. 3 and 4). These results are consistent with a previous report

on cells with deregulated CDT1 activity showing an increase in ssDNA gaps and DSBs together with longer fiber tracts[55], and a recent study showing that cells depleted of Geminin frequently undergo discontinuous DNA synthesis in a process mediated by RAD51 and the PrimPol primase[81]. Moreover, we were able to reproduce the phenotypes associated with high levels of ssDNA gaps and DNA damage in Geminin-depleted cells treated with Olaparib (Fig. 4 and Supplementary Figure 7). This is in line with the notion that PARP inhibitors increase fork speed and promote the accumulation of post-replicative ssDNA gaps[57-59] and with a recent study demonstrating a function for FANCM in supporting resistance to PARP inhibitors by minimizing formation of ssDNA gaps[85].

The mechanism of synthetic lethality caused by the accumulation of ssDNA lesions in re-replicating cells proposed here also supports the "fork-chasing-fork" model of re-replication[86], in which the leading strand of a re-replicating fork creates a DSB when reaching the un-ligated Okazaki fragment of an earlier fork. This mechanism was initially proposed as an alternative to the classical "head-to-tail" collision model born from studies in organisms with a high density of adjacent origins like *X. laevis* egg extracts[17,84]. Our results strengthen the idea that in large-size genomes, fork breakage upon re-replication does not necessarily require a head-to-tail fork collision. Rather, it might occur as forks reach ssDNA gaps nearby replication origins or upstream regions as a result of nucleolytic processing. The chasing fork model has been supported by studies in yeast and human cells linking formation of re-replicated repeat DNA sequences to gene amplifications and copy number variations[79,85]. As cancer cells frequently exhibit alterations in gene copy-number, our findings raise the question of whether modulating ssDNA accumulation during replication could serve as a strategy to selectively target cancer cells.

Our study also showed that FANCD2 is recruited at the vicinity of re-replicating forks after Geminin loss (Fig. 3 and Supplementary Figure 5). One possibility is that FANCD2 binds directly to the replisome as a mechanism of replication fork surveillance mediated by ATR. In line with this, FANCD2 has been shown to interact with the MCM helicase to ensure firing of an adequate number of licensed origins[89]. Also, cells with a decreased number of licensed origins constitutively activate the FA pathway[90], suggesting that FA signaling is necessary during normal S phase progression. Furthermore, FANCD2 also interacts with MCM proteins in response to replication stress, where it restricts new origin firing and prevents uncontrolled fork progression and accumulation of ssDNA gaps[54]. An alternative and non-mutually exclusive possibility is that FANCD2 clamps directly onto DNA at stalled forks of re-replicating cells to control nucleolytic processing ahead of the gap thus restoring canonical fork architecture and restart. Supporting this notion, recent observations have demonstrated that the FANCD2-FANCDI complex diffuses

along double-stranded DNA and pauses upon detection of ssDNA gaps at the ss–dsDNA junction of stalled forks[88,89]. Moreover, FANCD2 cooperates with BLM and MRE11 to restart stalled forks while FANCD2-deficient cells exhibit high levels of MRE11-mediated fork degradation under replication stress conditions[48,50,90].

Interestingly, timely association on nascent DNA from re-replicating forks was recently reported for the fork protection and DSB repair factor RAD51[81]. RAD51 limits the levels of re-replication and hinders the progression of re-replicating forks by promoting fork reversal prior to PrimPol-mediated repriming and MRE11-dependent fork restart[81]. Moreover, earlier work had suggested that FA signaling and FANCD2 activation are required for RAD51 foci formation and checkpoint activation upon re-replication[53]. Although we did not assess the effect in fiber length or fork reversal of co-depleting RAD51 in double Geminin and FANCD2-depleted cells, we showed that FANCD2 loss does not affect the levels of re-replication in Geminin-deficient cells (Fig. 3c and Supplementary Figure 6a), pointing to a different mechanism for maintaining stability at re-replicating forks. On these lines, recent studies have shown that FANCD2 modulates nucleosome mobility and stabilizes the RAD51-DNA complex to inhibit nucleolytic degradation and stimulate its strand exchange activity at stalled forks[50,91,92]. It is plausible that FANCD2 could at least partially regulate RAD51 function at nascent DNA of re-replicating forks by promoting transient fork reversal at ssDNA gaps prior to nucleolytic processing. In this scenario, the unrestrained activity of replisomes together with repriming and nucleolytic processing in double Geminin and FANCD2-deficient cells would result in the accumulation of long stretches of ssDNA.

A relevant part of our study relied on exploring the dynamics of mild re-replication through the genome-wide distribution of FANCD2 on chromatin. Previous studies showed that replication stress promotes accumulation of FANCD2 at the main body of large-transcribed genes in order to facilitate replication through CFSs and limit stretches of under-replicated DNA[62,63,93]. However, our data demonstrate that re-replication upon Geminin depletion induces FANCD2 recruitment at the promoter region of actively transcribed genes (Fig. 6). In sharp contrast to the features associated with difficult-to-replicate CFSs, often late-replicating and with a scarcity of origins[97], FANCD2-enriched genes of re-replicating cells are short, GC-rich and highly transcribed, and largely colocalize with early firing origins thus likely reflecting ERFSs, as evidenced by high overlap with defined ERFs in mice (Fig. 6 and 7)[76]. These results are consistent with recent evidence showing that clustered early-replicating origins are preferred for massive re-replication[77], and support genome-wide mapping of DNA replication origins in human cells next to TTS of actively transcribed genes[98-100].

A preferred use of early firing origins for re-replication most likely reflects the accessible chromatin conformation of these euchromatic regions, as it has been proposed to explain the uneven distribution of MCMs during DNA licensing[77,98]. An open chromatin would also facilitate high transcription of gene clusters at these early replicating regions. In this sense, our genome-wide analyses reveal increased R-loop levels at FANCD2-enriched genes. According to FANCD2 function in promoting fork stability by limiting R-loop accumulation[62,99,100], our results show that transcription inhibition and R-loop removal by incubation with RNAseH1 reduce DNA damage in Geminin-depleted cells (Fig. 7), supporting that active transcription is a key determinant in the genomic instability phenotypes associated with re-replication. Interestingly, TRCs have been observed upon oncogene-activation, in which intragenic origins are fired[69,101]. Given that re-replicating cells show a higher frequency of initiation from proximate origins[77], the clustered distribution of early firing origins could also contribute to TRCs and R-loop accumulation in re-replicating cells. This might be connected with the association between the activity of origins and the release of short fragments of re-replicated DNA[105], which could also explain the specific recruitment of FANCD2 at ERFSs observed in re-replicating cells. In any case, we cannot exclude the possibility that concomitantly to increased initiation events at ERFSs, re-replication also induces a paucity of replication at CFSs, challenging the completion of DNA duplication at such regions. Indeed, instability at both ERFS and CFS has been observed in oncogene-induced models of replication stress presenting defects in DNA licensing[101,103,104], which could be associated with copy number variations and chromosomal alterations of re-replicating cells.

In summary, the consequences of aberrant origin licensing have been traditionally monitored upon massive levels of re-replication which ultimately result in deleterious levels of DNA breaks that lead to senescence. However, mild levels of re-replication could escape detection by the cell cycle checkpoints, becoming a feature of malignant transformation. Along this line, Geminin deletion promotes carcinogenesis *in vivo* and increases the number and grade of tumors in mice cancer models[33]. Importantly, the increased fork fragility occurring upon re-activation of replication origins in the presence of ssDNA gaps uncovered in this study provides clues to the mechanisms connecting re-replication to genome evolution and tumorigenesis that could help seeking for alternative strategies for selective targeting of cancer cells.

Methods

Cell lines and drug treatment

All cell lines were grown at 37°C under standard cell culture conditions (humidified atmosphere, 5% CO2) and regularly tested for the detection of potential contamination with mycoplasma.

U2OS, MCF7, 293T and GMNN^{mAID} HCT116 cells were incubated in Dulbecco's modified Eagle's medium (DMEM) (Gibco™, 11962) supplemented with 10% heat inactivated fetal bovine serum (FBS). Human hTERT-RPE1 cells were grown in DMEM-F12 (Sigma-Aldrich, D8437), supplemented with 10% FBS. MCF10A cells were grown in DMEM-F12 supplemented with 5% horse serum, 20 ng/ml EGF, 0.5 µg/ml hydrocortisone, 10 µg/ml insulin and 100 ng/ml cholera toxin. K562, PD20 FANCD2-KO and PD20 FANCD2-WT cells were cultured in RPMI (Gibco™, 11875093) supplemented with 10% FBS. The following compounds were used in this manuscript at the indicated final concentrations unless stated otherwise: Hydroxyurea (1 mM, Sigma-Aldrich, H8627), Caffeine (5 mM, Sigma-Aldrich, C0750), VE-821 (ATRi, 2 µM, Sigma-Aldrich, SML1415), Olaparib (PARPi, 0,5 µM, Selleckchem, S1060), Aphidicolin (0,5 µM, Sigma-Aldrich, A0781), Nocodazole (100 ng/ml, Sigma-Aldrich, M1404), Cordycepin (100µM, Sigma-Aldrich C3394).

Generation of stable CDT1-GFP hTERT-RPE1 cells

To generate a CDT1-GFP stable cell line, hTERT-RPE1 cells were infected with lentiviral particles expressing GFP-NLS or CDT1-GFP. The second-generation lentiviral packaging plasmid mix was used for lentivirus production as previously described[105]. Briefly, 293T cells were co-transfected using Turbofect (Fermentas) with the expression vector carrying either GFP-NLS (pLVDest-GFP) or CDT1-GFP (pLVDest-CDT1-GFP) and the plasmids encoding for the structural proteins of the virus (psPAX2, Addgene 12260) and the proteins of the viral envelope (pMD2.G, Addgene 12259). The supernatant was harvested 48hs after transfection, filtered and used to infect hTERT-RPE1 cells with 5µg/mL of hexadimethrine bromide (polybrene, Sigma-Aldrich). Limiting dilution and single colony picking were used to generate stable cell lines.

Generation of inducible Geminin knockdown cell lines

To generate a U2OS cell line with doxycycline-inducible depletion of Geminin, shRNA sequences targeting human Geminin (GMNN) were cloned into the Tet-pLKO-puro "all-in-one" lentiviral system for tetracycline-inducible shRNA expression (Addgene #21915). shRNA sequences were selected from the RNAi Consortium collection (MISSION®, Sigma-Aldrich) and synthesized oligonucleotides for each shRNA were annealed and ligated into the Tet-pLKO-puro vector following enzimatic digestion followed by transformation into competent bacteria. Lentiviral particles were produced by co-transfecting HEK-293T cells with the individual shRNA-containing Tet-pLKO-puro plasmids, along with the packaging plasmids psPAX2 (Addgene #12260) and pMD2.G (Addgene #12259), using a suitable transfection reagent. Viral supernatant was collected 48 hours post-transfection, filtered through a 0.45 µm filter, and stored at -80°C. To generate

stable cell lines, U2OS cells were transduced with the lentiviral particles in the presence of 5 µg/ml Polybrene for 48 hours before selection and maintainance in media containing 2 µg/ml puromycin and Tet-System Approved FBS. To induce Geminin knockdown, stable cells were treated with 1µg/ml doxycycline for 48 hours.

Generation of mAID-tagged HCT116 cells

For the generation of the HCT116-Gem-mAID auxin inducible degron cells, the mAID tag was added in the C-terminal of the GMNN protein. Guide RNAs targeting the 3' UTR of the GMNN (Geminin) gene were designed with Bbs1/Bpi1 overhangs and ligated into pX330-U6-Chimeric_BB-CBh-hSpCas9 (#42230, Addgene). Homology directed repair templates were assembled using the GeneArt™ Gibson Assembly HiFi Master Mix (Invitrogen): ~900bp homology arms flanking the GMNN 3' UTR overwriting the stop codon, either mAID-mClover-Hygro or mAID-mCherry-NeoR pieces and the respective backbones cut by BamHI-HF from plasmids #72828 and #72830 (Addgene), respectively. Plasmids expressing the Cas9 and the targeted gRNAs and plasmids expressing the homology arms and the mAID cassettes were transfected into HCT116-CMV-OsTIR1 cells using FuGENE-HD (Promega) according to manufacturer's instructions. 24 hours after transfection cells were reseeded in low density and grown in antibiotics (Hygromycin 100 µg/ml, G418 700 µg/ml and Puromycin 2 µg/ml) for >10 days for colonies formation. Single colonies were selected and propagated independently. Correct clones were confirmed for the presence of the mAID cassette, the fluorescent markers, and the expression of the tagged protein by PCR, immunofluorescence microscopy and immunoblotting (in-house developed Geminin-specific antibodies).

Immunostaining

Immunofluorescence experiments were performed 72 hours after siRNA or plasmid transfection, unless otherwise indicated in the experiment. Optionally, for the detection of proteins closely bound to chromatin, cells were pre-extracted with 0,2% Triton X-100 in PBS for 2 mins at RT. Cells were fixed in 4% paraformaldehyde (PFA) solution for 10 mins at RT, washed three times in PBS, permeabilized with 0,3% Triton X-100 for 5 mins at RT and washed three times in PBS. Cells were then incubated with a blocking buffer containing PBS, 10% FBS and 3% BSA for 1 hour at RT, before incubation with primary antibodies for 16 hours at 4^{o}C in a humid chamber. After washed with PBS-0,1%Tween, coverslips were incubated with secondary antibodies for 1 hour at 25^{o}C in a dark and humid chamber. After three subsequent washes with PBS-0,1%Tween, coverslips were incubated with Hoechst 33342 for 15 mins at RT for nuclei staining. Finally, cells

were washed with PBS and mounted with MOWIOL® 4-88. (Sigma-Aldrich). A list of the antibodies used in this study can be found in Supplementary Data 1.

EdU labeling

5-Ethynyl-20-deoxyuridine (EdU, Invitrogen, Cat#C10340) labelling was performed using BaseClick EdU-HTS 488 kits (Sigma-Aldrich, Cat#BCK-HTS488-2). First, cells were cultured in complete medium supplemented with 10μM EdU for 30 mins at 37ºC. Optionally, to detect proteins closely bound to chromatin cells were treated with a pre-extraction solution (0,2% Triton X-100) for 2 mins at RT. Cells were then fixed by incubation with a 4% paraformaldehyde (PFA) solution for 10 mins at RT. After that, cells were washed for 3 subsequent times with 1xPBS for 5 mins each and then were permeabilized by incubation with a 0,3% Triton X-100 solution for 5 mins at RT. At this point, detection of EdU was performed on the coverslips according to manufacturer's instructions.

Detection of nascent ssDNA by native BrdU assay

To detect nascent ssDNA, native BrdU assay was performed as previously described[109]. Briefly, U2OS cells in coverslips, were pulse-labeled with 10 μM BrdU (Sigma-Aldrich, B5002) for 24 hours. After washing with PBS, cells were permeabilized with freshly made extraction buffer (10 mM PIPES, 100 mM NaCl, 300 mM sucrose, 1,5 mM MgCl2 and 0,5% Triton X-100) for 2 mins on ice. Subsequently, cells were fixed with 4% PFA for 10 mins on ice and washed 3 times in PBS. Cells were then incubated with a blocking buffer containing PBS and 10% FBS for 1 hour at RT, before incubation with mouse monoclonal anti-BrdU (B44 clone) (BD Biosciences, 347580, 1:50) for 16 hours at 4ºC in a humid chamber. After washing with PBS, coverslips were incubated with goat anti-mouse secondary antibody (Life Technologies, A11031) for 1 hour at 25ºC in a dark and humid chamber. After three subsequent washes with PBS, coverslips were incubated with Hoechst 33342 for 15 mins at RT for nuclei staining. Finally, cells were washed with PBS and mounted with MOWIOL ® 4-88 (Sigma-Aldrich).

Cell synchronization for monitoring DNA synthesis along S and G2

For synchronization of U2OS cells to monitor DNA synthesis along S and G2, cells were plated onto coverslips and incubated with 2mM of thymidine (Sigma-Aldrich, T9250) for 20 hours, then washed 2 times with 1xPBS and released in normal media for an additional period of 6 hours. During the release period, cells were transfected with a siRNA oligo targeting Geminin or against a control sequence, as mentioned above. 5 hours after transfection, the medium was removed,

and cells were incubated with 10 μM of CDK1 inhibitor RO-3306 (Sigma-Aldrich, SML0569) for 8h. Cells were then washed 2 times with 1xPBS and were subsequently released for 12 hours prior to collection of timepoints every 2h for a total time-course of 30 hours. 30 mins before each timepoint, cells were incubated with 10 μM EdU (Invitrogen, Cat#C10340) to monitor replication. Fixed cells were then permeabilized and immunofluorescence analyses coupled with EdU detection were performed, as mentioned above.

PLA assay

PLA was performed using Duolink PLA Technology (Merck). Cells were incubated with 25mM EdU for 15 mins. Samples were then incubated with 0.1% formaldehyde in PBS for 5 mins, and pre-extracted in CSK buffer (10 mM Pipes pH 7, 0.1 M NaCl, 0.3 M sucrose and 3 mM MgCl2), prior to fixation. Click Reaction (100 mM Tris-HCl pH 8, 100 mM CuSO4, 20 mg/mL sodium-L-ascorbate and 10mM azide-biotin) was performed according to the manufacturer's instructions for 30 mins at 37ºC. Duolink Blocking Solution was replaced by 5% BSA, 10% Donkey serum in PBS. First and secondary antibody binding, ligation and amplification reactions were performed according to the manufacturer's instructions. The PLA reaction was performed using the following reagents: PCNA (PC10, sc-56, Santa Cruz), MCM2 (D7G11, 3619, Cell Signaling), FANCD2 (NB100-182, Novus Biologicals), anti-Biotin (200-002-211, Jackson ImmunoResearch), Duolink in situ PLA probe anti-rabbit PLUS (Merck, DUO92002), Duolink in situ PLA probe anti-mouse MINUS (Merck, DUO92004) and Duolink-Detection Reagents Red (Merck). Finally, nuclei were stained with DAPI and mounted with MOWIOL® 4-88. (Sigma-Aldrich). Antibodies were used at 1:500 dilution. PLA foci were automatically quantified using Metamorph v7.5.1.0 software (Molecular Probes).

Flow Cytometry

For 2D EdU/PI flow cytometry, cells were pulse-labeled with 10 μM EdU for 30 min before harvest. Afterwards, cells were trypsinized, washed in PBS, resuspended in 70% ice-cold ethanol and optionally stored at 4˚C. Cells were then washed with PBS 1% BSA and incubated with 0,5% Triton X-100 in PBS for 10 mins. EdU staining was performed using the BaseClick EdU-HTS 488 kit (Sigma-Aldrich, BCK-HTS488-2) according to the manufacturer's instructions. The genomic DNA was stained with propidium iodide (Biotium, 40017) in combination with RNAse (AppliChem, A2760). For Annexin V/PI flow cytometry Annexin V Apoptosis Detection Kit (BD Pharmingen™, 556547) was used, according to manufacturer's instructions. A BD FACSCantoTM Flow

Cytometry System with FACSDiva software was used and FlowJo10 was used for cell cycle analysis.

siRNA transfections

Transient gene depletions were carried out using the Lipofectamine RNAiMax transfection reagent, according to the manufacturer's instructions, and a final concentration of 20 nM, unless stated otherwise. Silencer select negative control #1 siRNA was used as a control siRNA at the same concentration of the most concentrated siRNA used in the same experiment. For each experiment, cells were plated at approximately 70-80% confluency in 35mm dishes. Cells were incubated with the mixture of Opti-MEM, RNAiMax and siRNA for 5h at 37 ^{o}C and then the transfection medium was removed and full DMEM 10% FBS was added to cells. Control over transfection efficiency was monitored 24h – 48h post-transfection by Western Blot (WB) analysis. The following Silencer Select siRNAs were used: siGMNN (s27306), siFANCD2 (s533670), siFANCA (s528717), siCDT1 (s37722).

siRNA-based high content screening

Phenotypic image-based siRNA screens were performed in 384-well format as previously described[110]. Briefly, a custom designed siRNA library consisting of three individual siRNAs targeting 300 DNA repair genes (Silencer Select, Thermo Fisher Scientific, Supplementary Data 1) was pre-printed into 384 wells. From stock siRNA libraries, in which every well contained a single-targeting siRNA oligo at a concentration of 0.16μM, 5μl per well were transferred onto screening plates with the use of a multichannel pipette, in which a mixture of 5μl of Opti-MEM and 0.09μl of RNAiMAX was then added. Lipid mixture was incubated with the siRNAs for 20 mins at RT and 40μl of cells in suspension at a concentration of $1x10^3$ cells per well were then added to the lipid mixture to reach a final concentration of siRNA of 16nM in a total volume of 50μl. Cells were incubated with the transfection solution for 48hs and before fixation staining of cells. During automated high-content screening, a total of 9 pictures per well were acquired for the analysis of over 1000 cells using a 20x air lens using an Olympus ScanR wide-field microscope equipped with DAPI, FITC, Cy3 and Cy5 filters. Automated image quantification and analysis were performed in the ScanR station software (Olympus ScanR Image Analysis Software version 3.0.0 & 3.0.1) based on mean intensities of fluorescent signal. The analysis pipeline used the DAPI channel for the detection of the nuclei and the application of a mask that served to quantify pixel intensities for EdU incorporation and γH2AX for each individual cell. ScanR data was processed in Excel for heatmap generation, normalization of systematic plate effects and calculation of

percentage of negative controls. For analysis of significance and hit identification based on γH2AX and EdU, positive cells or mean intensity values were normalized for systematic plate (column-wise "CNORM") effects prior to calculate the percentage of control values and standardize these values by robust Z-score transformation. For analysis of cell counts, raw values were used to calculate the percentage of control and robust Z-score transformation. Only siRNAs with a mean z-score ± 2 standard deviations to negative controls were considered significant. To ensure on-target specificity, a candidate was selected as a true hit only if a z-score greater than 2 was achieved by a minimum of two out of three individual siRNA oligos.

Plasmid transfection

Transient transfections of plasmid DNA were carried out using the Lipofectamine 2000 transfection reagent, according to the manufacturers' instructions, and a final concentration of 1 µg/ml of the corresponding plasmid DNA. For each experiment, cells were plated at approximately 70-80% confluency in 35mm dishes. Cells were incubated with the mixture of Opti-MEM, Lipofectamine 2000 and plasmid DNA for 5h at 37ºC and then the transfection medium was removed and full DMEM 10% FBS was added to cells. Control over transfection efficiency was monitored 24 hours – 48 hours post-transfection through fluorescence-microscopy (IF) and by Western Blot (WB) analysis.

DNA fiber assay and S1 nuclease DNA fiber assay

For experiments with siRNA treatment and drug treatment, exponentially growing cells were pulse-labeled with 25 µM IdU (5-Iodo-2'-deoxyuridine, Millipore Sigma) for 30 min, washed 3 times with pre-warmed PBS, then pulse-labeled with 250 µM CldU (5-Chloro-2'-deoxyuridine, Millipore Sigma) for 30 minutes, followed by 3 washes with cold PBS. Cells were harvested, pelleted at approximately 300 x g for 5 mins at 4ºC, and resuspended in PBS for a final concentration of $7{,}5*10^5$ cells/ml. For the DNA fiber assay with the ssDNA-specific S1 nuclease, cells were permeabilized with CSK100 (100 mM NaCl, 10 mM MOPS pH 7, 3 mM MgCl2, 300 mM sucrose and 0.5% Triton X-100 in water) after the CldU pulse for 10 mins at R.T., washed once with PBS and then treated with the S1 nuclease (18001-016, Thermo Fisher Scientific) at 20 U/mL in Nuclease S1 buffer for 30 mins at 37°C, and collected in PBS-0.1% BSA with cell scraper. Nuclei were then pelleted at 4600 x g for 5 mins at 4^0C, then resuspended in PBS (nuclei cannot be quantified, so initial number of cells plated should be considered when resuspending to a final concentration of 1,500 nuclei/µl).

For both the standard DNA fiber assay and the S1 fiber assay, 6 µl of cells were mixed with 7 µl of lysis buffer (200 mM Tris-HCl pH 7.5, 50 mM EDTA, 0.5% SDS in water) on top of a positively charged glass slide, pre-coated with a freshly prepared solution of methanol: glacial acetic acid at 3:1 for 10 mins. After 3 mins incubation at RT, slides were tilted at 15-20 angle to spread the fibers at a constant, low speed. After air drying for 10-15 mins at RT, DNA was fixed onto the slides with a freshly prepared solution of methanol: glacial acetic acid at 3:1 for 5 min, dried, and stored at 4°C overnight. For immuno-staining of DNA fibers, DNA was denatured with 2,5 M HCl for 80 mins at RT. Slides were then washed with PBS three times and blocked with 5% BSA at RT for 20 mins. DNA fibers were immuno-stained against BrdU (1:400, Bu1/75 Ab6326, Abcam and 1:25, 347580, BD Biosciences) for 2 hours at RT, washed 3 times with PBS for 5 mins each, and then incubated with stringency buffer (10 mM Tris-HCl pH 7, 400 mM NaCl, 0,02% Tween, 0,02% NP-40) for 10 mins. After 3 washes with PBS of 5 mins each, DNA fibers were incubated with anti-rat Alexa Fluor 488 (1:750, A21470) and anti-mouse Alexa Fluor 546 (1/1000, A21123) and then washed 3 times with PBS, for 5 mins each, before mounting with 100 µl Mowiol®. Images were acquired using the LAS AF software using TCS SP5 confocal microscope (Leica) with a 63x oil immersion objective and each experiment was repeated at least two times independently. At least 15 images were taken across the whole slide using only one channel to select the regions for the images, to avoid any potential bias. Al least 100-150 individual tracts were scored for each data set. For all DNA fiber experiments, we measured both IdU and CldU tracts only on forks characterized by contiguous IdU-CldU signals. The length of each tract was measured manually using the straight-line tool on ImageJ software. Pixel values were converted into µm using the scale bar generated by the microscope software. Size distribution of tract lengths or ratios from individual DNA fibers were plotted as scatter dot plots with the center line representing the median. Data were pooled from independent experiments. Statistical differences in DNA fiber tract lengths were determined by the Mann-Whitney U test.

Chromatin fractionation

Cells were scrapped from the surface of the plate with ice-cold PBS and 1:3 of the volume was kept as total protein isolates (WCE), boiled for 5 mins at 95ºC and stored at -80ºC until further analysis. Samples were centrifuged for 5 mins at 500g at 4ºC and the supernatant was discarded and replaced by 100µl of Buffer A (10mM Hepes pH=7.9, 10mM KCl, 1.5mM MgCl2, 340mM Sucrose, 10% Glycerol, 1mM DTT, 0.1%Triton X-100, 1xProtease inhibitor cocktail - Complete EDTA-free). Samples were then centrifuged for 5 mins at 500g at 4ºC and the supernatant was transferred to new tubes and stored in FSB-DTT as the cytoplasmic fraction. Samples pellets

were then resuspended in 75µl of Buffer B and kept on ice for 10 mins before being centrifuged for 5 mins at 1700g at 4ºC. The supernatant was transferred to new tubes and stored in FSB-DTT as the nuclear fraction. Insoluble chromatin was collected by washing cell pellets with 50µl of Buffer B (5mM Hepes pH=7.9, 3mM EDTA, 0.2mM EGTA, 1mM DTT, 1xProtease inhibitor cocktail - Complete EDTA-free) and by sonication at 6 cycles of 5s ON/OFF and 30% amplitude before adding FSB-DTT.

Western blotting

Cells were cultured in 35mm dishes and whole cell extracts were obtained by lysis of pelleted cells in 1xFSB-dTT. Samples were boiled at 95°C for 5 mins and centrifuged at 4°C for 5 mins at 15.500 g. Lysates were loaded in a 4%-20% SDS gel, according to each experiment with the use of a marker for the molecular weight (MWP04, Nippon Genetics), following standard procedures. After the protein separation proteins were then transferred from the polyacrylamide gel to an Immobilon-P PVDF membrane (Millipore, IPVH00010) using a wet blotting system (Biorad). Membrane sections were blocked for 1 hour at RT using a blocking buffer containing 5% milk in PBS – 0,1% Tween, unless used for the immunodetection of p-Chk1 or Chk1, when the membrane was blocked with a blocking buffer containing 3% BSA in 1xPBS – 0,1% Tween. Primary antibodies were incubated for 16 hours at RT in blocking buffer. Membranes were washed thoroughly with PBS - 0,1% Tween (2 quick washes, 1x15min, 3x5min), before incubation with secondary HRP-conjugated antibodies for 1 hour at RT. Membranes were washed again with 1xPBS - 0,1% Tween (2 quick washes, 1x15min, 3x5min) and bound antibodies were detected through a chemiluminescent reaction with the use of Clarity™ ECL, by using the ChemiDoc imaging system (Biorad). A list of the antibodies used in this study can be found in Supplementary Information. Uncropped scans are provided in the Source Data.

Clonogenic assays

For cell survival assays, after the specific treatment was performed, cells were seeded onto 6-well plates in technical triplicates for each condition (750-1000 cells per well). Cells were cultured for 10-14 days, with a change of media in-between, before fixation with the fixative solution (0,5% crystal violet, 20% methanol in water). Percentage of survival was measured by manual colony counting after methanol/0.5% crystal violet staining.

RNA isolation, reverse transcription, and quantitative PCR (qPCR)

Total RNA was extracted from cells using the NucleoSpin RNA kit (740955.50, Macherey-Nagel) according to manufacturers' instructions. cDNA was synthesized by M-MLV Reverse Transcriptase (28025013, Invitrogen) and PCR was performed using 10 ng of cDNA as a template, using the KAPA SYBR® FAST qPCR reagent kit (KapaBiosystems) in a StepOne™ Real-Time PCR System (Applied Biosystems) according to manufacturers' instructions. The results were calculated according to the 2-ΔΔCt methodology and are shown as relative expressions to the correspondent control. Results were then analyzed using the REST-MCS beta software.

Metaphase spreads

Mitotic cells were collected by incubation with 100ng/ml Nocodazole for 12hours at 37ºC and mitotic shake-off. After centrifugation, cell pellets were incubated in a hypotonic solution (0.075M KCl) for 20 mins at 37ºC and fixed in a freshly prepared mix of methanol:acetic acid (3:1). For chromosome spreading, nuclear preparations were dropped onto pre-fixed slides and stained with DAPI. Image acquisition was performed using a Nikon Eclipse TE 2000-U or Olympus IX83 widefield microscopes at 63x magnification. An appropriate number of metaphase spreads were imaged so to have representative numbers for subsequent analyses on the number of DNA fragments and chromosomal aberrations. After image acquisition, chromosomes were analyzed using ImageJ/Fiji to account for DNA fragments, chromosome breaks or abnormal chromosome structures. Only metaphase spreads clearly isolated were analyzed.

Chromatin immunoprecipitation ChIP

For chromatin immunoprecipitation (ChIP-qPCR), 1-2×10^7 cells were transfected with the indicated siRNAs for 48 hours and were then fixed by incubation in 1% formaldehyde for 10 mins at RT. Fixed cells were then quenched with 200mM glycine, washed in PBS and frozen at -80ºC for later processing. Lysates were generated by serial incubation of cell pellets in lysis buffers and chromatin was sheared by sonication using a Bioruptor Pico sonicator (Thermo Fisher Scientific) until the average sheared size was 500bp. Sheared chromatin was then cleared by high-speed centrifugation and used for immunoprecipitation (IP). For each IP, 40µl of Protein A Dynabeads (Thermo) were washed, blocked in PBS+0.5% BSA and conjugated with 1µg of anti-FANCD2 or anti-IgG and then incubated with 30µg of cleared, sonicated lysate. Beads were washed three times in RIPA buffer and DNA was eluted, de-crosslinked and purified for qPCR analysis in order to validate the assay. Reactions were run using Universal SYBR Green Supermix (Bio-Rad), and

all qPCRs were performed using a PCR 7500 Fast reader (primers used are available upon request). The dilution factor was adjusted, and the percentage of the input signal was calculated.

ChIP-seq and genome-wide data analysis

After ChIP was conducted using the standard protocol, sequencing libraries were built using the ThruPLEX DNA-Seq Kit (Takara Bio) and size-checked with a Bioanalyzer DNA High sensitive chip. Samples were then sequenced in a NextSeq500 Illumina platform using a 2x75bp paired-end read high output flow cell with high success (92.91 % >=Q30). Sequencing data were first subjected to quality control filtering, demultiplexing and adapter trimming using the BaseSpace Seq Hub from Illumina. Downstream processing of ChIP-seq data was performed using the European Galaxy Platform v18.05-20.05 (https://usegalaxy.eu), UNIX command line (GNU bash, version 4.2.46(2)) and R studio (2022.07.0 Build 548) with R 4.2.1 version; Reads were mapped to the canonical version of human reference genome hg38 (H. sapiens, GRCh38 no-alt analysis set; (https://bowtie-bio.sourceforge.net/bowtie2/manual.shtml) with Bowtie2[111] and further processed using SAMtools[112] (up to Galaxy Version 2.0.3 / UNIX 1.9). PCR duplicates were removed and only properly paired primary alignments with a mapping quality (MAPQ) > 20 used for downstream analysis. Coverage data were computed using RPKM normalization for each file with deepTools[109] (up to Galaxy Version 3.3.2.0.0 / UNIX 3.5.1). Then, mean coverages from the two biological replicates were calculated and the Input subtracted from IP signal, for better visualization of the results. Peak calling was performed with MACS2 package[114] (up to Galaxy Version 2.1.1.20160309.6) allowing broad peak identification (--broad option) and setting p-value and broad cutoffs < 0.01. Biological replicates were then intersected using BEDtools[115] (up to Galaxy Version 2.29.2 / UNIX 2.29.2) and only peaks detected in both replicates considered for further analysis. Comparative analysis was conducted using BEDtools to determine condition-specific peaks (only appearing in one condition). We used HOMER[112] (UNIX v4.11) for standard genome annotation of the peak datasets with the default annotation dataset and a homemade annotation dataset to cross the peak datasets with genome features of our interest: common fragile sites (CFS), centromeres and telomeres (retrieved from UCSC), rDNA, R-loops[79] and DNA replication origins[66]. We applied contingency tests to calculate $\log_2$ odds ratios and evaluate the statistical significance of differences between conditions. We crossed peaks with chromatin features retrieved from UCSC[118] (bedGraphToBigWig) (UNIX v4) by intersecting genomic regions using BEDtools. Geecee package[118] was used to calculate GC content. Integrative Genome Viewer (IGV)[119] (v2.15.2) for visualize genome-wide data and deepTools for metaplot analysis. Additional genome-wide tracks used in this work were retrieved from sources as determined

in[121,122], except K562 Repli-Seq data which was obtained from the ENCODE project (Replication Timing Series: ENCSR591OXO) and average coverage of Repli-seq data from each S subphases measured at specific sites using deepTools. Human ERFSs were inferred by lifting over ERFS data from synchronized mouse B cells data using LiftOver (UCSC)[121] (Kent, W.J., Sugnet, C.W., Furey, T.S., Roskin, K.M., Pringle, T.H., Zahler, A.M., & Haussler, D. (2002). The Human Genome Browser at UCSC. Genome Research, 12(6), 996-1006. DOI:10.1101/gr.229102), as previously done[76].

TCGA data analysis

Data were accessed through the public TCGA data portal and the cBioPortal for Cancer Genomics (http://www.cbioportal.org). For each cancer type, samples with both expression and CNA data were divided in quartiles based on the mRNA expression of CDT1. FANCD2 expression was assessed in tumors with high CDT1 expression (samples in the first quartile of the CDT1 distribution) and high CDT1 expression (samples in the fourth quartile).

Image acquisition, statistics, and reproducibility

Images obtained from immunofluorescence experiments, DNA fibers and metaphase spreads were acquired with Nikon Eclipse TE2000-U, an Olympus IX83 inverted widefield microscope or a Leica TCS SP5 confocal scanning microscope. Acquisition of images for colocalization assays and EdU incorporation was performed using a Leica TCS SP5 confocal scanning microscope. Images were analyzed with ImageJ/FIJI software (64-bit, National Healthcare Institute, USA). Statistical analysis and graphs were generated using Graph Pad Prism version 7 or 9 and Metamorph (Molecular Devices). Statistical significances (p values) of the observed differences between conditions are indicated in figure panels and figure legends.

Data Availability

ChIP-seq data have been deposited in NCBI's Gene Expression Omnibus with GEO Series accession number GSE285033 [https://www.ncbi.nlm.nih.gov/geo/query/acc.cgi?acc=GSE285033]. The analysis of the Microscopy data is available at Zenodo (https://doi.org/10.5281/zenodo.18000043). Raw image files and reagents are available from the corresponding author. Source data are provided with this paper.

Code availability

The custom ImageJ/Fiji and Cell Profiler macros used for the analysis of nuclear areas, signal intensity, foci quantification, and colocalization have been deposited in GitHub (https://github.com/ElenaKarydi/Image-analysis-pipelines/releases/tag/v1.0.0).

References

1 Rhind, N. & Gilbert, D. M. DNA Replication Timing. *Cold Spring Harbor Perspectives in Biology* **5**, a010132-a010132 (2013). https://doi.org/10.1101/cshperspect.a010132

2 Marks, A. B., Fu, H. & Aladjem, M. I. Regulation of Replication Origins. *Adv Exp Med Biol* **1042**, 43-59 (2017). https://doi.org/10.1007/978-981-10-6955-0_2

3 Ticau, S. *et al.* Mechanism and timing of Mcm2-7 ring closure during DNA replication origin licensing. *Nat Struct Mol Biol* **24**, 309-315 (2017). https://doi.org/10.1038/nsmb.3375

4 Li, J. *et al.* The human pre-replication complex is an open complex. *Cell* **186**, 98-111.e121 (2023). https://doi.org/10.1016/j.cell.2022.12.008

5 Reuter, L. M. *et al.* MCM2-7 loading-dependent ORC release ensures genome-wide origin licensing. *Nat Commun* **15**, 7306 (2024). https://doi.org/10.1038/s41467-024-51538-9

6 Ticau, S., Friedman, L. J., Ivica, N. A., Gelles, J. & Bell, S. P. Single-molecule studies of origin licensing reveal mechanisms ensuring bidirectional helicase loading. *Cell* **161**, 513-525 (2015). https://doi.org/10.1016/j.cell.2015.03.012

7 Yang, R., Hunker, O., Wise, M. & Bleichert, F. Multiple mechanisms for licensing human replication origins. *Nature* (2024). https://doi.org/10.1038/s41586-024-08237-8

8 Symeonidou, I.-E., Taraviras, S. & Lygerou, Z. Control over DNA replication in time and space. *FEBS Letters* **586**, 2803-2812 (2012). https://doi.org/10.1016/j.febslet.2012.07.042

9 Fragkos, M., Ganier, O., Coulombe, P. & Méchali, M. DNA replication origin activation in space and time. *Nat Rev Mol Cell Biol* **16**, 360-374 (2015). https://doi.org/10.1038/nrm4002

10 Aparicio, T., Guillou, E., Coloma, J., Montoya, G. & Méndez, J. The human GINS complex associates with Cdc45 and MCM and is essential for DNA replication. *Nucleic Acids Res* **37**, 2087-2095 (2009). https://doi.org/10.1093/nar/gkp065

11 Ratnayeke, N., Baris, Y., Chung, M., Yeeles, J. T. P. & Meyer, T. CDT1 inhibits CMG helicase in early S phase to separate origin licensing from DNA synthesis. *Mol Cell* **83**, 26-42.e13 (2023). https://doi.org/10.1016/j.molcel.2022.12.004

12 Hiraga, S. I. *et al.* Human RIF1 and protein phosphatase 1 stimulate DNA replication origin licensing but suppress origin activation. *EMBO Rep* **18**, 403-419 (2017). https://doi.org/10.15252/embr.201641983

13 Ticau, S., Larry, Nikola, Gelles, J. & Stephen. Single-Molecule Studies of Origin Licensing Reveal Mechanisms Ensuring Bidirectional Helicase Loading. *Cell* **161**, 513-525 (2015). https://doi.org/10.1016/j.cell.2015.03.012

14 Zhang, H. Regulation of DNA Replication Licensing and Re-Replication by Cdt1. *Int J Mol Sci* **22** (2021). https://doi.org/10.3390/ijms22105195

15 Kiang, L., Heichinger, C., Watt, S., Bähler, J. & Nurse, P. Specific replication origins promote DNA amplification in fission yeast. *Journal of Cell Science* **123**, 3047-3051 (2010). https://doi.org/10.1242/jcs.067470

16 Thomer, M., May, N. R., Aggarwal, B. D., Kwok, G. & Calvi, B. R. Drosophila double-parkedis sufficient to induce re-replication during development and is regulated by cyclin E/CDK2. *Development* **131**, 4807-4818 (2004). https://doi.org/10.1242/dev.01348

17 Davidson, I. F., Li, A. & Blow, J. J. Deregulated Replication Licensing Causes DNA Fragmentation Consistent with Head-to-Tail Fork Collision. *Molecular Cell* **24**, 433-443 (2006). https://doi.org/10.1016/j.molcel.2006.09.010

18 Liontos, M. *et al.* Deregulated overexpression of hCdt1 and hCdc6 promotes malignant behavior. *Cancer Res* **67**, 10899-10909 (2007). https://doi.org/10.1158/0008-5472.Can-07-2837

19 Galanos, P. *et al.* Chronic p53-independent p21 expression causes genomic instability by deregulating replication licensing. *Nat Cell Biol* **18**, 777-789 (2016). https://doi.org/10.1038/ncb3378

20 Muñoz, S. *et al.* In Vivo DNA Re-replication Elicits Lethal Tissue Dysplasias. *Cell Rep* **19**, 928-938 (2017). https://doi.org/10.1016/j.celrep.2017.04.032

21 Petropoulos, M. *et al.* <scp>Cdt1</scp> overexpression drives colorectal carcinogenesis through origin overlicensing and <scp>DNA</scp> damage. *The Journal of Pathology* **259**, 10-20 (2023). https://doi.org/10.1002/path.6017

22 Petropoulou, C. Cdt1 and Geminin in cancer: markers or triggers of malignant transformation? *Frontiers in Bioscience* **Volume**, 4485 (2008). https://doi.org/10.2741/3018

23 Vanderdys, V. *et al.* The Neddylation Inhibitor Pevonedistat (MLN4924) Suppresses and Radiosensitizes Head and Neck Squamous Carcinoma Cells and Tumors. *Molecular Cancer Therapeutics* **17**, 368-380 (2018). https://doi.org/10.1158/1535-7163.mct-17-0083

24 Yoshimura, C. *et al.* TAS4464, A Highly Potent and Selective Inhibitor of NEDD8-Activating Enzyme, Suppresses Neddylation and Shows Antitumor Activity in Diverse Cancer Models. *Mol Cancer Ther* **18**, 1205-1216 (2019). https://doi.org/10.1158/1535-7163.Mct-18-0644

25 Pozo, P. & Cook, J. Regulation and Function of Cdt1; A Key Factor in Cell Proliferation and Genome Stability. *Genes* **8**, 2 (2016). https://doi.org/10.3390/genes8010002

26 De Marco, V. *et al.* Quaternary structure of the human Cdt1-Geminin complex regulates DNA replication licensing. *Proc Natl Acad Sci U S A* **106**, 19807-19812 (2009). https://doi.org/10.1073/pnas.0905281106

27 Dimaki, M. *et al.* Cell cycle-dependent subcellular translocation of the human DNA licensing inhibitor geminin. *J Biol Chem* **288**, 23953-23963 (2013). https://doi.org/10.1074/jbc.M113.453092

28 McGarry, T. J. & Kirschner, M. W. Geminin, an inhibitor of DNA replication, is degraded during mitosis. *Cell* **93**, 1043-1053 (1998). https://doi.org/10.1016/s0092-8674(00)81209-x

29 Tada, S., Li, A., Maiorano, D., Méchali, M. & Blow, J. J. Repression of origin assembly in metaphase depends on inhibition of RLF-B/Cdt1 by geminin. *Nat Cell Biol* **3**, 107-113 (2001). https://doi.org/10.1038/35055000

30 Zhu, W. & Depamphilis, M. L. Selective killing of cancer cells by suppression of geminin activity. *Cancer Res* **69**, 4870-4877 (2009). https://doi.org/10.1158/0008-5472.Can-08-4559

31 Shreeram, S., Sparks, A., Lane, D. P. & Blow, J. J. Cell type-specific responses of human cells to inhibition of replication licensing. *Oncogene* **21**, 6624-6632 (2002). https://doi.org/10.1038/sj.onc.1205910

32 Petropoulos, M., Champeris Tsaniras, S., Taraviras, S. & Lygerou, Z. Replication Licensing Aberrations, Replication Stress, and Genomic Instability. *Trends Biochem Sci* **44**, 752-764 (2019). https://doi.org/10.1016/j.tibs.2019.03.011

33 Champeris Tsaniras, S. *et al.* Geminin ablation in vivo enhances tumorigenesis through increased genomic instability. *J Pathol* **246**, 134-140 (2018). https://doi.org/10.1002/path.5128

34 Kalogeropoulou, A. *et al.* Intrinsic neural stem cell properties define brain hypersensitivity to genotoxic stress. *Stem Cell Reports* **17**, 1395-1410 (2022). https://doi.org/10.1016/j.stemcr.2022.04.018

35 Karantzelis, N. *et al.* Small Molecule Inhibitor Targeting CDT1/Geminin Protein Complex Promotes DNA Damage and Cell Death in Cancer Cells. *Frontiers in Pharmacology* **13** (2022). https://doi.org/10.3389/fphar.2022.860682

36 Pappas, K. *et al.* BRCA2 reversion mutation-independent resistance to PARP inhibition through impaired DNA prereplication complex function. *Proc Natl Acad Sci U S A* **122**, e2426743122 (2025). https://doi.org/10.1073/pnas.2426743122

37 Semlow, D. R. & Walter, J. C. Mechanisms of Vertebrate DNA Interstrand Cross-Link Repair. *Annual Review of Biochemistry* **90**, 107-135 (2021). https://doi.org/10.1146/annurev-biochem-080320-112510

38 Badra Fajardo, N., Taraviras, S. & Lygerou, Z. Fanconi anemia proteins and genome fragility: unraveling replication defects for cancer therapy. *Trends Cancer* **8**, 467-481 (2022). https://doi.org/10.1016/j.trecan.2022.01.015

39 Zhu, W., Chen, Y. & Dutta, A. Rereplication by Depletion of Geminin Is Seen Regardless of p53 Status and Activates a G₂/M Checkpoint. *Molecular and Cellular Biology* **24**, 7140-7150 (2004). https://doi.org/10.1128/mcb.24.16.7140-7150.2004

40 O'Connell, M. J., Raleigh, J. M., Verkade, H. M. & Nurse, P. Chk1 is a wee1 kinase in the G2 DNA damage checkpoint inhibiting cdc2 by Y15 phosphorylation. *Embo j* **16**, 545-554 (1997). https://doi.org/10.1093/emboj/16.3.545

41 Sørensen, C. S. & Syljuåsen, R. G. Safeguarding genome integrity: the checkpoint kinases ATR, CHK1 and WEE1 restrain CDK activity during normal DNA replication. *Nucleic Acids Res* **40**, 477-486 (2012). https://doi.org/10.1093/nar/gkr697

42 Panagopoulos, A., Taraviras, S., Nishitani, H. & Lygerou, Z. CRL4(Cdt2): Coupling Genome Stability to Ubiquitination. *Trends Cell Biol* **30**, 290-302 (2020). https://doi.org/10.1016/j.tcb.2020.01.005

43 Lee, J. & Zhou, P. DCAFs, the missing link of the CUL4-DDB1 ubiquitin ligase. *Mol Cell* **26**, 775-780 (2007). https://doi.org/10.1016/j.molcel.2007.06.001

44 Kawasaki, T. *et al.* BCL2L2 is a probable target for novel 14q11.2 amplification detected in a non-small cell lung cancer cell line. *Cancer Sci* **98**, 1070-1077 (2007). https://doi.org/10.1111/j.1349-7006.2007.00491.x

45 Natsume, T., Kiyomitsu, T., Saga, Y. & Kanemaki, M. T. Rapid Protein Depletion in Human Cells by Auxin-Inducible Degron Tagging with Short Homology Donors. *Cell Reports* **15**, 210-218 (2016). https://doi.org/10.1016/j.celrep.2016.03.001

46 Thakur, B. L., Ray, A., Redon, C. E. & Aladjem, M. I. Preventing excess replication origin activation to ensure genome stability. *Trends Genet* **38**, 169-181 (2022). https://doi.org/10.1016/j.tig.2021.09.008

47 Ceccaldi, R., Sarangi, P. & D'Andrea, A. D. The Fanconi anaemia pathway: new players and new functions. *Nat Rev Mol Cell Biol* **17**, 337-349 (2016). https://doi.org/10.1038/nrm.2016.48

48 Schlacher, K., Wu, H. & Jasin, M. A Distinct Replication Fork Protection Pathway Connects Fanconi Anemia Tumor Suppressors to RAD51-BRCA1/2. *Cancer Cell* **22**, 106-116 (2012). https://doi.org/10.1016/j.ccr.2012.05.015

49 Kais, Z. *et al.* FANCD2 Maintains Fork Stability in BRCA1/2-Deficient Tumors and Promotes Alternative End-Joining DNA Repair. *Cell Rep* **15**, 2488-2499 (2016). https://doi.org/10.1016/j.celrep.2016.05.031

50 Liu, W. *et al.* FANCD2 and RAD51 recombinase directly inhibit DNA2 nuclease at stalled replication forks and FANCD2 acts as a novel RAD51 mediator in strand exchange to promote genome stability. *Nucleic Acids Res* **51**, 9144-9165 (2023). https://doi.org/10.1093/nar/gkad624

51 Alexander, J. L., Barrasa, M. I. & Orr-Weaver, T. L. Replication fork progression during re-replication requires the DNA damage checkpoint and double-strand break repair. *Curr Biol* **25**, 1654-1660 (2015). https://doi.org/10.1016/j.cub.2015.04.058

52 Lin, J. J. & Dutta, A. ATR Pathway Is the Primary Pathway for Activating G2/M Checkpoint Induction After Re-replication. *Journal of Biological Chemistry* **282**, 30357-30362 (2007). https://doi.org/10.1074/jbc.m705178200

53 Zhu, W. & Dutta, A. An ATR- and BRCA1-mediated Fanconi anemia pathway is required for activating the G2/M checkpoint and DNA damage repair upon rereplication. *Mol Cell Biol* **26**, 4601-4611 (2006). https://doi.org/10.1128/mcb.02141-05

54 Lossaint, G. *et al.* FANCD2 binds MCM proteins and controls replisome function upon activation of s phase checkpoint signaling. *Mol Cell* **51**, 678-690 (2013). https://doi.org/10.1016/j.molcel.2013.07.023

55 Neelsen, K. J. *et al.* Deregulated origin licensing leads to chromosomal breaks by rereplication of a gapped DNA template. *Genes & Development* **27**, 2537-2542 (2013). https://doi.org/10.1101/gad.226373.113

56 Luis *et al.* ATR Prohibits Replication Catastrophe by Preventing Global Exhaustion of RPA. *Cell* **155**, 1088-1103 (2013). https://doi.org/10.1016/j.cell.2013.10.043

57 Maya-Mendoza, A. *et al.* High speed of fork progression induces DNA replication stress and genomic instability. *Nature* **559**, 279-284 (2018). https://doi.org/10.1038/s41586-018-0261-5

58 Cong, K. *et al.* Replication gaps are a key determinant of PARP inhibitor synthetic lethality with BRCA deficiency. *Molecular Cell* **81**, 3128-3144.e3127 (2021). https://doi.org/10.1016/j.molcel.2021.06.011

59 Machacova, Z., Chroma, K., Lukac, D., Protivankova, I. & Moudry, P. DNA polymerase α-primase facilitates PARP inhibitor-induced fork acceleration and protects BRCA1-deficient cells against ssDNA gaps. *Nat Commun* **15**, 7375 (2024). https://doi.org/10.1038/s41467-024-51667-1

60 Thompson, E. L. *et al.* FANCI and FANCD2 have common as well as independent functions during the cellular replication stress response. *Nucleic Acids Research* **45**, 11837-11857 (2017). https://doi.org/10.1093/nar/gkx847

61 Raghunandan, M., Chaudhury, I., Kelich, S. L., Hanenberg, H. & Sobeck, A. FANCD2, FANCJ and BRCA2 cooperate to promote replication fork recovery independently of the Fanconi Anemia core complex. *Cell Cycle* **14**, 342-353 (2015). https://doi.org/10.4161/15384101.2014.987614

62 Chen, X., Bosques, L., Sung, P. & Kupfer, G. M. A novel role for non-ubiquitinated FANCD2 in response to hydroxyurea-induced DNA damage. *Oncogene* **35**, 22-34 (2016). https://doi.org/10.1038/onc.2015.68

63 Zhou, B. *et al.* Comprehensive, integrated, and phased whole-genome analysis of the primary ENCODE cell line K562. *Genome Research* **29**, 472-484 (2019). https://doi.org/10.1101/gr.234948.118

64 Madireddy, A. *et al.* FANCD2 Facilitates Replication through Common Fragile Sites. *Mol Cell* **64**, 388-404 (2016). https://doi.org/10.1016/j.molcel.2016.09.017

65 Okamoto, Y. *et al.* FANCD2 protects genome stability by recruiting RNA processing enzymes to resolve R-loops during mild replication stress. *Febs j* **286**, 139-150 (2019). https://doi.org/10.1111/febs.14700

66 Picard, F. *et al.* The spatiotemporal program of DNA replication is associated with specific combinations of chromatin marks in human cells. *PLoS Genet* **10**, e1004282 (2014). https://doi.org/10.1371/journal.pgen.1004282
67 Chen, Y.-H. *et al.* Transcription shapes DNA replication initiation and termination in human cells. *Nature Structural & Molecular Biology* **26**, 67-77 (2019). https://doi.org/10.1038/s41594-018-0171-0
68 Buratowski, S. Progression through the RNA Polymerase II CTD Cycle. *Molecular Cell* **36**, 541-546 (2009). https://doi.org/10.1016/j.molcel.2009.10.019
69 Abe, K., Schauer, T. & Torres-Padilla, M. E. Distinct patterns of RNA polymerase II and transcriptional elongation characterize mammalian genome activation. *Cell Rep* **41**, 111865 (2022). https://doi.org/10.1016/j.celrep.2022.111865
70 Local, A. *et al.* Identification of H3K4me1-associated proteins at mammalian enhancers. *Nature Genetics* **50**, 73-82 (2018). https://doi.org/10.1038/s41588-017-0015-6
71 Shoaib, M. *et al.* Histone H4K20 methylation mediated chromatin compaction threshold ensures genome integrity by limiting DNA replication licensing. *Nature Communications* **9** (2018). https://doi.org/10.1038/s41467-018-06066-8
72 Macheret, M. & Halazonetis, T. D. Intragenic origins due to short G1 phases underlie oncogene-induced DNA replication stress. *Nature* **555**, 112-116 (2018). https://doi.org/10.1038/nature25507
73 Audit, B. *et al.* Open chromatin encoded in DNA sequence is the signature of 'master' replication origins in human cells. *Nucleic Acids Research* **37**, 6064-6075 (2009). https://doi.org/10.1093/nar/gkp631
74 Cayrou, C. *et al.* The chromatin environment shapes DNA replication origin organization and defines origin classes. *Genome Research* **25**, 1873-1885 (2015). https://doi.org/10.1101/gr.192799.115
75 Hansen, R. S. *et al.* Sequencing newly replicated DNA reveals widespread plasticity in human replication timing. *Proceedings of the National Academy of Sciences* **107**, 139-144 (2010). https://doi.org/10.1073/pnas.0912402107
76 Barlow, J. H. *et al.* Identification of Early Replicating Fragile Sites that Contribute to Genome Instability. *Cell* **152**, 620-632 (2013). https://doi.org/10.1016/j.cell.2013.01.006
77 Mortusewicz, O., Herr, P. & Helleday, T. Early replication fragile sites: where replication–transcription collisions cause genetic instability. *The EMBO Journal* **32**, 493-495 (2013). https://doi.org/10.1038/emboj.2013.20
78 Pang, B., de Jong, J., Qiao, X., Wessels, L. F. A. & Neefjes, J. Chemical profiling of the genome with anti-cancer drugs defines target specificities. *Nat Chem Biol* **11**, 472-480 (2015). https://doi.org/10.1038/nchembio.1811
79 Bayona-Feliu, A., Barroso, S., Muñoz, S. & Aguilera, A. The SWI/SNF chromatin remodeling complex helps resolve R-loop-mediated transcription–replication conflicts. *Nature Genetics* **53**, 1050-1063 (2021). https://doi.org/10.1038/s41588-021-00867-2
80 Fu, H. *et al.* Dynamics of replication origin over-activation. *Nat Commun* **12**, 3448 (2021). https://doi.org/10.1038/s41467-021-23835-0
81 Lin, J. J., Milhollen, M. A., Smith, P. G., Narayanan, U. & Dutta, A. NEDD8-Targeting Drug MLN4924 Elicits DNA Rereplication by Stabilizing Cdt1 in S Phase, Triggering Checkpoint Activation, Apoptosis, and Senescence in Cancer Cells. *Cancer Research* **70**, 10310-10320 (2010). https://doi.org/10.1158/0008-5472.can-10-2062
82 Green, B. M., Finn, K. J. & Li, J. J. Loss of DNA Replication Control Is a Potent Inducer of Gene Amplification. *Science* **329**, 943-946 (2010). https://doi.org/10.1126/science.1190966
83 Finn, K. J. & Li, J. J. Single-stranded annealing induced by re-initiation of replication origins provides a novel and efficient mechanism for generating copy number expansion via non-

allelic homologous recombination. *PLoS Genet* **9**, e1003192 (2013). https://doi.org/10.1371/journal.pgen.1003192

84 Muñoz, S. *et al.* RAD51 restricts DNA over-replication from re-activated origins. *Embo j* **43**, 1043-1064 (2024). https://doi.org/10.1038/s44318-024-00038-z

85 Liu, Z., Jiang, H., Lee, S. Y., Kong, N. & Chan, Y. W. FANCM promotes PARP inhibitor resistance by minimizing ssDNA gap formation and counteracting resection inhibition. *Cell Reports* **43**, 114464 (2024). https://doi.org/10.1016/j.celrep.2024.114464

86 Alexander, J. L. & Orr-Weaver, T. L. Replication fork instability and the consequences of fork collisions from rereplication. *Genes Dev* **30**, 2241-2252 (2016). https://doi.org/10.1101/gad.288142.116

87 Blow, J. J., Gillespie, P. J., Francis, D. & Jackson, D. A. Replication origins in Xenopus egg extract Are 5-15 kilobases apart and are activated in clusters that fire at different times. *J Cell Biol* **152**, 15-25 (2001). https://doi.org/10.1083/jcb.152.1.15

88 Nathanailidou, P. *et al. Aberrant replication licensing drives Copy Number Gains across species* (Cold Spring Harbor Laboratory, 2020).

89 Panneerselvam, J. *et al.* Basal level of FANCD2 monoubiquitination is required for the maintenance of a sufficient number of licensed-replication origins to fire at a normal rate. *Oncotarget* **5**, 1326-1337 (2014). https://doi.org/10.18632/oncotarget.1796

90 Luebben, S. W., Kawabata, T., Johnson, C. S., O'Sullivan, M. G. & Shima, N. A concomitant loss of dormant origins and FANCC exacerbates genome instability by impairing DNA replication fork progression. *Nucleic Acids Research* **42**, 5605-5615 (2014). https://doi.org/10.1093/nar/gku170

91 Alcón, P. *et al.* FANCD2-FANCI is a clamp stabilized on DNA by monoubiquitination of FANCD2 during DNA repair. *Nat Struct Mol Biol* **27**, 240-248 (2020). https://doi.org/10.1038/s41594-020-0380-1

92 Alcón, P. *et al.* FANCD2–FANCI surveys DNA and recognizes double- to single-stranded junctions. *Nature* **632**, 1165-1173 (2024). https://doi.org/10.1038/s41586-024-07770-w

93 Chaudhury, I., Sareen, A., Raghunandan, M. & Sobeck, A. FANCD2 regulates BLM complex functions independently of FANCI to promote replication fork recovery. *Nucleic Acids Res* **41**, 6444-6459 (2013). https://doi.org/10.1093/nar/gkt348

94 Higgs, M. R. *et al.* Histone Methylation by SETD1A Protects Nascent DNA through the Nucleosome Chaperone Activity of FANCD2. *Mol Cell* **71**, 25-41.e26 (2018). https://doi.org/10.1016/j.molcel.2018.05.018

95 Sato, K. *et al.* FANCI-FANCD2 stabilizes the RAD51-DNA complex by binding RAD51 and protects the 5'-DNA end. *Nucleic Acids Res* **44**, 10758-10771 (2016). https://doi.org/10.1093/nar/gkw876

96 Pentzold, C. *et al.* FANCD2 binding identifies conserved fragile sites at large transcribed genes in avian cells. *Nucleic Acids Research* **46**, 1280-1294 (2018). https://doi.org/10.1093/nar/gkx1260

97 Debatisse, M. & Rosselli, F. A journey with common fragile sites: From S phase to telophase. *Genes Chromosomes Cancer* **58**, 305-316 (2019). https://doi.org/10.1002/gcc.22704

98 Dellino, G. I. *et al.* Genome-wide mapping of human DNA-replication origins: levels of transcription at ORC1 sites regulate origin selection and replication timing. *Genome Res* **23**, 1-11 (2013). https://doi.org/10.1101/gr.142331.112

99 Karnani, N., Taylor, C. M., Malhotra, A. & Dutta, A. Genomic study of replication initiation in human chromosomes reveals the influence of transcription regulation and chromatin structure on origin selection. *Mol Biol Cell* **21**, 393-404 (2010). https://doi.org/10.1091/mbc.e09-08-0707

100 Chen, Y. H. *et al.* Transcription shapes DNA replication initiation and termination in human cells. *Nat Struct Mol Biol* **26**, 67-77 (2019). https://doi.org/10.1038/s41594-018-0171-0

101 Mei, L., Kedziora, K. M., Song, E. A., Purvis, J. E. & Cook, J. G. The consequences of differential origin licensing dynamics in distinct chromatin environments. *Nucleic Acids Res* **50**, 9601-9620 (2022). https://doi.org/10.1093/nar/gkac003

102 Liang, Z. *et al.* Binding of FANCI-FANCD2 Complex to RNA and R-Loops Stimulates Robust FANCD2 Monoubiquitination. *Cell Rep* **26**, 564-572.e565 (2019). https://doi.org/10.1016/j.celrep.2018.12.084

103 García-Rubio, M. L. *et al.* The Fanconi Anemia Pathway Protects Genome Integrity from R-loops. *PLoS Genet* **11**, e1005674 (2015). https://doi.org/10.1371/journal.pgen.1005674

104 Jones, R. M. *et al.* Increased replication initiation and conflicts with transcription underlie Cyclin E-induced replication stress. *Oncogene* **32**, 3744-3753 (2013). https://doi.org/10.1038/onc.2012.387

105 Gómez, M. & Antequera, F. Overreplication of short DNA regions during S phase in human cells. *Genes Dev* **22**, 375-385 (2008). https://doi.org/10.1101/gad.445608

106 Tsantoulis, P. K. *et al.* Oncogene-induced replication stress preferentially targets common fragile sites in preneoplastic lesions. A genome-wide study. *Oncogene* **27**, 3256-3264 (2008). https://doi.org/10.1038/sj.onc.1210989

107 Brison, O. *et al.* Mistimed origin licensing and activation stabilize common fragile sites under tight DNA-replication checkpoint activation. *Nat Struct Mol Biol* **30**, 539-550 (2023). https://doi.org/10.1038/s41594-023-00949-1

108 Arbi, M. *et al.* GemC1 controls multiciliogenesis in the airway epithelium. *EMBO Rep* **17**, 400-413 (2016). https://doi.org/10.15252/embr.201540882

109 Kilgas, S., Kiltie, A. E. & Ramadan, K. Immunofluorescence microscopy-based detection of ssDNA foci by BrdU in mammalian cells. *STAR Protoc* **2**, 100978 (2021). https://doi.org/10.1016/j.xpro.2021.100978

110 Mäkelä, R. *et al.* Ex vivo analysis of DNA repair targeting in extreme rare cutaneous apocrine sweat gland carcinoma. *Oncotarget* **12**, 1100-1109 (2021). https://doi.org/10.18632/oncotarget.27961

111 Langmead, B. & Salzberg, S. L. Fast gapped-read alignment with Bowtie 2. *Nature Methods* **9**, 357-359 (2012). https://doi.org/10.1038/nmeth.1923

112 Li, H. *et al.* The Sequence Alignment/Map format and SAMtools. *Bioinformatics* **25**, 2078-2079 (2009). https://doi.org/10.1093/bioinformatics/btp352

113 Ramírez, F. *et al.* deepTools2: a next generation web server for deep-sequencing data analysis. *Nucleic Acids Res* **44**, W160-165 (2016). https://doi.org/10.1093/nar/gkw257

114 Zhang, Y. *et al.* Model-based analysis of ChIP-Seq (MACS). *Genome Biol* **9**, R137 (2008). https://doi.org/10.1186/gb-2008-9-9-r137

115 Quinlan, A. R. & Hall, I. M. BEDTools: a flexible suite of utilities for comparing genomic features. *Bioinformatics* **26**, 841-842 (2010). https://doi.org/10.1093/bioinformatics/btq033

116 Bayona-Feliu, A., Barroso, S., Muñoz, S. & Aguilera, A. The SWI/SNF chromatin remodeling complex helps resolve R-loop-mediated transcription-replication conflicts. *Nat Genet* **53**, 1050-1063 (2021). https://doi.org/10.1038/s41588-021-00867-2

117 Ernst, J. *et al.* Mapping and analysis of chromatin state dynamics in nine human cell types. *Nature* **473**, 43-49 (2011). https://doi.org/10.1038/nature09906

118 Rice, P., Longden, I. & Bleasby, A. EMBOSS: the European Molecular Biology Open Software Suite. *Trends Genet* **16**, 276-277 (2000). https://doi.org/10.1016/s0168-9525(00)02024-2

119 Robinson, J. T. *et al.* Integrative genomics viewer. *Nat Biotechnol* **29**, 24-26 (2011). https://doi.org/10.1038/nbt.1754

120 Bayona-Feliu, A. *et al.* The chromatin network helps prevent cancer-associated mutagenesis at transcription-replication conflicts. *Nat Commun* **14**, 6890 (2023). https://doi.org/10.1038/s41467-023-42653-0

121 Kent, W. J. *et al.* The human genome browser at UCSC. *Genome Res* **12**, 996-1006 (2002). https://doi.org/10.1101/gr.229102

Acknowledgements

We thank the Advanced Light Microscopy facility at the Medical School of the University of Patras for their support with experiments, the University of Patras for financial support, and the members of our groups for insightful discussions. We are also grateful to Dr. Raphael Ceccaldi for sharing the PD20 cells, Dr. Bert van de Kooij for sharing the FANCD2-KO and corrected U2OS cells and Vassilis Roukos for scientific advice in the generation of the mAID-Geminin HCT116 cells. This study was supported by research funding from the European Union Horizon 2020 research and innovation program under the Marie Sklodowska-Curie grant agreement No. 722729, the European Union Horizon Europe (2021-2027), "ESPERANCE" ERA Chair program (GA 101087215), the Hellenic Foundation for Research and Innovation (H.F.R.I.) under the “2nd Call for H.F.R.I. Research Projects to support Faculty Members & Researchers” (Project Number: 2728) and project TAEDR-0539180 implemented within the framework of “Actions in interdisciplinary scientific areas with special interests for the connection with the productive fabric", Greece 2.0 - National Recovery and Resilience Plan to Z.L. N.B.F. received fellowships from the Federation of European Biochemical Societies (FEBS) and the Operational Programme «Human Resources Development, Education and Lifelong Learning 2014- 2020» (IKY). This work was also funded by grants from the Spanish Agencia Estatal de Investigación (PID2022-138251NB-I00 funded by MCIN/AEI/10.13039/501100011033 “ERDF A way of making Europe”) and the Caixa Research Foundation (LCF/PR/HR22/52420014) to A.A.

Author contributions

Conceptualization, N.B.F., and Z.L.; Methodology, N.B.F., A.B.F., B.G.G., J.K.R., S.T., A.A. and Z.L.; Investigation, N.B.F., E.K., M.A. and A.K.; Data analysis, N.B.F., E.K., A.B.F. and O.P.; Writing of original draft, review & editing, N.B.F., B.G.G., A.A. and Z.L.; Supervision, S.T., A.A. and Z.L.

Competing interests

Juha K. Rantala is the founder of Misvik Biology Oy. All remaining authors declare no competing interests.

Figure legends

Fig. 1: High-content siRNA screening identifies FANCD2 as essential to prevent DNA damage in re-replicating cells. a. Schematic of the screen; hTERT-RPE1 cells were transfected with control or Geminin siRNAs and the designed siRNA library prior to EdU pulse, fixation and immunostaining for γH2AX. Nuclei were also stained with DAPI. Analyses were based on mean intensities and robust z-score transformation in respect to negative controls. **b.** Left: Mean robust z-scores of γH2AX intensities and total cell counts for Geminin-depleted cells. Right: Top ranked genes in the Geminin-depleted cell model and corresponding values in control cells for γH2AX nuclear intensities and total cell counts. **c.** Top: Immunoblot detection of indicated proteins in hTERT-RPE1 cells transfected with indicated siRNAs. α-Tubulin, loading control. Bottom: Images and quantification of transfected hTERT-RPE1 cells stained for γH2AX (left) and 53BP1 (right). For γH2AX intensities, data pooled from n=3 biological replicates (> 250 cells per condition and replicate); two-tailed Mann-Whitney U test, ****p < 0.0001, ns = not significant. For cells with >10 53BP1 foci, plot shows mean ± SD of n=4 biological replicates (> 250 cells per condition and replicate); two-tailed unpaired t-test, ***p = 0,0007, **p = 0,0054, *p = 0.0120, ns = not significant. **d.** Schematic of the workflow, representative images and quantification of long-term clonogenic assays in hTERT-RPE1 cells transfected with indicated siRNAs. Plot shows mean ± SD of n=3 biological replicates; two-tailed unpaired t-test, ****p < 0.0001, ***p = 0.0003, *p = bottom to top; 0.0177, 0.0158. DNA staining, Hoechst. Scale bar, 10μm. siCtrl, negative siRNA control; siGMNN, siRNA targeting Geminin; siFANCD2, siRNA targeting FANCD2. Source data are provided as a Source Data file.

Fig. 2: FANCD2 is recruited at re-replicating forks prior to massive DNA breakage. a. Immunoblot of Geminin in whole-cell extracts, soluble, and chromatin fractions. α-Tubulin and H3 were used as loading controls. Quantification of Geminin in the chromatin fraction was normalized to loading and control samples. Plot shows mean ± SD of n=3 biological replicates; two-tailed unpaired t-test, **p = 0.0025. **b.** Top: Representative images and quantification of Geminin-depleted U2OS cells stained for γH2AX and FANCD2. For cells with >10 FANCD2 foci, plot shows mean ± SD of n=3 biological replicates (> 250 cells per condition and replicate); two-tailed unpaired t-test, **p = 0.0018. Bottom: Histogram of FANCD2 and γH2AX foci co-localization (yellow line on Hoechst). Plot shows colocalizing foci per nucleus for each condition; two-tailed Mann-Whitney U test, ****p < 0.0001. **c.** Left: Representative images of the kinetics of FANCD2 and γH2AX foci in Geminin-depleted U2OS cells. Right: Quantification of cells with >10 FANCD2 and γH2AX foci in Geminin-depleted U2OS cells during the time-course experiment. Plots show

mean ± SD of n=3 biological replicates (> 250 cells per condition and replicate); two-tailed unpaired t-test, ***p = 0.0009, **p = 0.0094 (FANCD2), **p = 0.0093 (γH2AX), *p = 0.0188, ns = not significant. **d.** Representative images of synchronized U2OS cells and quantification of EdU positive cells at indicated timepoints. Plots show mean of n=2 biological replicates (> 150 cells per condition and replicate). **e.** Representative images of Geminin-depleted U2OS cells pulse-labelled with EdU and stained for FANCD2 and RPA, together with quantification of cells with >10 FANCD2 foci (top) or >10 RPA foci (bottom) at indicated timepoints. Plots show data pooled from n=2 biological replicates (> 200 cells per condition and replicate); two-tailed Mann-Whitney U test, ****p < 0.0001, ***p = 0.0001, **p = 0.0077, *p = 0.0388, ns = not significant. DNA staining, Hoechst. Scale bar, 10µm. WCE, whole cell extract. Chr, chromatin. Source data are provided as a Source Data file.

Fig. 3: FANCD2 limits fork progression and genomic instability in Geminin-depleted cells upon checkpoint activation. a. Quantification of FANCD2-EdU PLA foci in transfected U2OS cells. Data pooled from n=3 biological replicates (> 200 cells per condition and replicate); two-tailed Mann-Whitney U test, ****p < 0.0001. **b.** Quantification of MCM2-FANCD2 PLA foci in transfected and EdU pulse-labelled cells (30 min). Data pooled from n=3 biological replicates (> 200 cells per condition and replicate); two-tailed Mann-Whitney U test, ****p < 0.0001. **c.** Flow cytometry analysis (PI vs EdU) showing cell cycle distribution of transfected cells. Cell cycle phase percentages are shown for a representative experiment (n=3 biological replicates). **d.** Quantification of nuclear areas in transfected cells. Data pooled from n=3 biological replicates (> 250 cells per condition and replicate); two-tailed Mann-Whitney U test, ****p < 0.0001. **e.** Representative images of DNA fibers and quantification of CldU length (left) and fork asymmetry (right) in transfected cells. Box plots show medians, 25th/75th percentiles (bounds), and 5th/95th percentiles (whiskers); dots, outliers. Data pooled from n=3 biological replicates (> 100 fibers per condition and replicate); two-tailed Mann-Whitney U test, ****p < 0.0001, *p = 0.0143. **f.** Percentage of origin firing in transfected cells. Mean ± SD of n=3 biological replicates (> 100 fibers per condition and replicate); two-tailed unpaired t-test, *p = 0.0393, ns, not significant. **g.** Quantification of transfected and EdU pulse-labelled cells (30 min) stained for PCNA and pH3. For pH3-positive cells, mean ± SD of n=4 biological replicates. For pH3/PCNA/EdU triple-positive cells, mean ± SD of n=2 biological replicates (> 200 cells per condition and replicate); two-tailed unpaired t-test. pH3-positive: ***p = 0.0006, **p = bottom to top; 0.0021, 0.0086, *p = 0.0443. pH3/PCNA/EdU triple-positive: **p = 0.0053 (siFANCD2 vs siGMNN+siFANCD2), *p = 0.0110 (siGMNN vs siGMNN+siFANCD2), 0.03650 (siCtrl vs siGMNN), ns = not significant (siCtrl vs

siFANCD2). **h.** Top: Immunoblot of indicated proteins; α-Tubulin, loading control. Bottom: Quantification of pChk1 levels. Mean ± SD of n=3 biological replicates; two-tailed unpaired t-test, ***p = bottom to top; 0.0002, 0.0008, **p = 0.0029, ns = not significant. DNA staining, Hoechst. Scale bar, 10μm. pH3, Histone H3-Ser10Pho; PLA, Proximity Ligation Assay. Source data are provided as a Source Data file.

Fig. 4: Loss of FANCD2 promotes the accumulation of ssDNA gaps and genomic instability in Geminin-depleted cells. a. RPA32 foci in transfected U2OS cells. Mean ± SD of n=3 biological replicates (>150 cells per condition and replicate); two-tailed unpaired t-test, ***p = 0.0002, **p = bottom to top; 0.0018, 0.0055, ns = not significant. **b.** Native BrdU foci. Mean ± SD of n=3 biological replicates (> 100 cells per condition and replicate); two-tailed unpaired t-test, **p = 0.0086, *p = bottom to top; 0.02, 0.0388, ns = not significant. **c.** Schematic of DNA fibers and total tract length (+ S1 nuclease, 30 min). Box plots show medians, 25th/75th percentiles (bounds), and 1st/99th percentiles (whiskers); dots, outliers. Data pooled from n=3 biological replicates (> 100 fibers per condition and replicate); two-tailed Mann-Whitney U test, **** p < 0.0001, ns = not significant. **d.** Top: Immunoblot of transfected cells + 0,5μM Olaparib (24hs). α-Tubulin, loading control. Bottom: Total fiber tract length in Geminin-depleted cells + Olaparib + S1 nuclease. Box plots as in c. Data pooled from n=3 biological replicates (> 100 fibers per condition and replicate); two-tailed Mann-Whitney U test, ****p < 0.0001, ns = not significant. **e.** RPA32 foci in cells treated as in d. Mean ± SD of n=3 biological replicates (> 200 cells per condition and replicate); two-tailed unpaired t-test, ****p < 0.0001, ***p = 0.0004, **p = 0.0013, *p = 0.0289. **f.** Chromosome fragments (left) and aberrations (right) per metaphase. Blue arrowheads, fragments; red, aberrations. Box plots show medians, 25th/75th percentiles (bounds), and 5th/95th percentiles (whiskers); dots, outliers. Data pooled from n=3 biological replicates (> 30 metaphases per condition and replicate); two-tailed Mann-Whitney U test, ****p < 0.0001, *p = 0.0142 (fragments), 0.0399 (aberrations), ns = not significant. **g.** Quantification of 53BP1 NBs (left) and MNs (right). Mean ± SD of n=3 biological replicates (> 250 cells per condition and replicate); two-tailed unpaired t-test. NBs: *p = bottom to top; 0.0102, 0.0180, 0.0484, ns = not significant. MNs: ***p = bottom to top; 0.0006, 0.0008, **p = 0.0022, *p = 0.0323. DNA staining, Hoechst. Scale bar, 10μm. NBs, nuclear bodies. MNs, micronuclei. Source data are provided as a Source Data file.

Fig. 5: Contribution of FANCD2 mono-ubiquitination to cell survival during re-replication. a. Immunoblot and quantification of indicated proteins in transfected U2OS cells. α-Tubulin,

loading control. Plot shows mean ± SD of n=3 biological replicates; two-tailed unpaired t-test, *p = 0.0287, ns = not significant. **b.** Quantification of γH2AX intensities and 53BP1 foci in transfected cells. For γH2AX intensities, data pooled from n=3 biological replicates (> 200 cells per condition and replicate; two-tailed Mann-Whitney U test, ****p < 0.0001. For cells with >10 53BP1 foci, mean ± SD of n=3 biological replicates (> 200 cells per condition and replicate); two-tailed unpaired t-test, ****p < 0.0001, ***p = 0.0006, ns = not significant. **c.** Quantification of RPA32 foci in transfected cells. For cells with >10 RPA32 foci, mean ± SD of n=3 biological replicates (> 200 cells per condition and replicate; two-tailed unpaired t-test, **p = bottom to top; 0.0026, 0.0011, *p = 0.0429, ns = not significant. For RPA foci intensities, plot shows a representative experiment from n=3 biological replicates (> 200 cells per condition and replicate); two-tailed Mann-Whitney U test, ****p < 0.0001. **d.** Long-term clonogenic assays of transfected cells. Mean ± SD of n=3 biological replicates; two-tailed unpaired t-test, ****p < 0.0001, **p = 0.0010, *p = 0.0321, ns = not significant. **e.** Quantification of FANCD2 foci in transfected cells. For cells with >10 FANCD2 foci, mean ± SD of n=3 biological replicates (> 200 cells per condition and replicate); two-tailed unpaired t-test, ***p = 0.0007, **p = 0.0032, *p = bottom to top; 0.0167, 0.0418. For FANCD2 foci intensities, plot shows a representative experiment from n=3 biological replicates (> 200 cells per condition and replicate); two-tailed Mann-Whitney U test, ****p < 0.0001. **f.** Immunoblot in FANCD2 KO and corrected (WT and K561R) U2OS cells transfected with indicated siRNAs. **g.** Long-term clonogenic assays of FANCD2 KO and corrected (WT and K561R) cells transfected with indicated siRNAs. Mean ± SD of n=3 biological replicates; two-tailed unpaired t-test, ****p < 0.0001, ***p = 0.0009, **p = 0.0034, *p = bottom to top; 0.0475, 0.0205, ns = not significant. DNA staining, Hoechst. Scale bar, 10μm. Source data are provided as a Source Data file.

Fig. 6: Genome-wide enrichment of FANCD2 at replication fork conflicts upon Geminin depletion. a. Representative screenshot of FANCD2-enriched regions in control (yellow), common (grey), and Geminin-depleted (blue) K562 cells. **b.** Metaplot of FANCD2 occupancy at peaks (±5kb) specific to control, Geminin-depleted or shared (common) conditions. **c.** Peak annotation to genomic features. Left: $\log_2$ enrichment and $-\log_{10}$ p-values. Right: differential enrichment between Geminin-depleted and control conditions. Contingency tests were used to calculate $\log_2$ odds ratios and evaluate statistical significances. **d.** Top: Venn diagram showing genome-wide co-localization of FANCD2-enriched genes in control and Geminin-depleted cells. Bottom: Gene length, CG content and expression levels of FANCD2-enriched genes in control and Geminin-depleted cells. Box plots show medians, 25th/75th percentiles (bounds), and 1st/99th percentiles (whiskers); dots, outliers. FANCD2-enriched genes were identified from

FANCD2 ChIP-seq data. P-values were calculated by chi-square test one-sided, one degree of freedom. **e.** Peak annotation across gene-associated features. Left: $\log_2$ enrichment and $-\log_{10}$ p-values. Right: differential enrichment between conditions. Contingency tests used as in c. **f.** BrdU intensity at origins enriched for FANCD2. Box plots show medians, 25th/75th percentiles (bounds), and 2.5th/97.5th percentiles (whiskers); dots, outliers. Profile represents average Repli-seq coverage (ENCODE) across FANCD2-enriched genomic sites. FANCD2-enriched loci represent a consensus set from two independent biological replicates of FANCD2 ChIP-seq; two-tailed Mann-Whitney U test, ****p < 0.0001, ns = not significant. Genome localization, scale bars and coverage tracks are indicated. CFSs, common fragile sites. UTR, untranslated region. TTS, transcription termination site. Source data are provided as a Source Data file.

Fig. 7: FANCD2 limits R-loop-associated fragility in Geminin-depleted cells. a. Metaplot of γH2AX ChIP-seq signal (±20 kb) of FANCD2-enriched genes. **b.** Metagene analysis of DRIPc-seq signal (±0.5 kb) in Geminin-depleted K562 cells. **c.** FANCD2 ChIP–seq mean signal at ERFs (±1 mb) in Geminin-depleted K562 cells. Arrow indicates sites of ERFSs accumulation. **d.** Quantification of γH2AX intensities, and FANCD2 and RPA32 foci in Geminin-depleted U2OS cells treated with 100μM Cordycepin (4hs). For γH2AX nuclear intensities, data pooled from n=3 biological replicates (> 150 cells per condition and replicate); two-tailed Mann-Whitney U test, ****p < 0.0001. For cells with >10 FANCD2/RPA32 foci, mean ± SD of n=3 biological replicates (> 250 cells per condition and replicate); two-tailed unpaired t-test, ****p < 0.0001, ***p = bottom to top; 0.0007, 0.0002, *p = left to right; 0.0477, 0.0469, ns = not significant. **e.** Quantification of γH2AX intensities, and FANCD2 and RPA32 foci in Geminin-depleted cells transfected with eGFP or RNAseH1-GFP (24hs). For γH2AX nuclear intensities, data pooled from n=3 biological replicates (> 150 cells per condition and replicate); two-tailed Mann-Whitney U test, **p = left to right; 0.0091, 0.0067, *p= 0.0461, ns = not significant. For cells with >10 FANCD2/RPA foci, mean ± SD of n=3 biological replicates (> 250 cells per condition and replicate); two-tailed unpaired t-test, ****p < 0.0001, **p = left to right; 0.0060, 0.0078, 0.0060, *p = left to right; 0.0394, 0.0393, ns = not significant. **f.** Model to explain fork fragility upon re-replication in Geminin-depleted cells. Re-firing of early origins located within highly transcribed genes promotes the accumulation of FANCD2 at re-replicating forks to limit their advancement, thereby preventing the accumulation of ssDNA gaps and collisions with the transcription machinery. In the absence of FANCD2, unrestrained replisome progression results in the generation of post-replicative ssDNA gaps that can be subsequently converted into DSBs by advancing re-replicating forks. Uncontrolled progression of re-replicating forks upon FANCD2 loss also leads to the accumulation of

transcription-replication conflicts and formation of R-loops, leading to fork fragility. DNA staining, Hoechst. Scale bar, 10μm. ERFs, early fragile sites, Cord., Cordycepin, RH1, RNaseH1. Source data are provided as a Source Data file.

Editorial Summary:
Re-replication is a driving force of tumorigenesis and genomic instability. Here, the authors show that upon re-replication, FANCD2 localizes at early origins to limit replisome progression, ssDNA gap accumulation and fork breakage, revealing a vulnerability for selective targeting of cancer cells.

Peer review information: *Nature Communications* thanks Corrado Santocanale and the other, anonymous, reviewer(s) for their contribution to the peer review of this work. A peer review file is available.

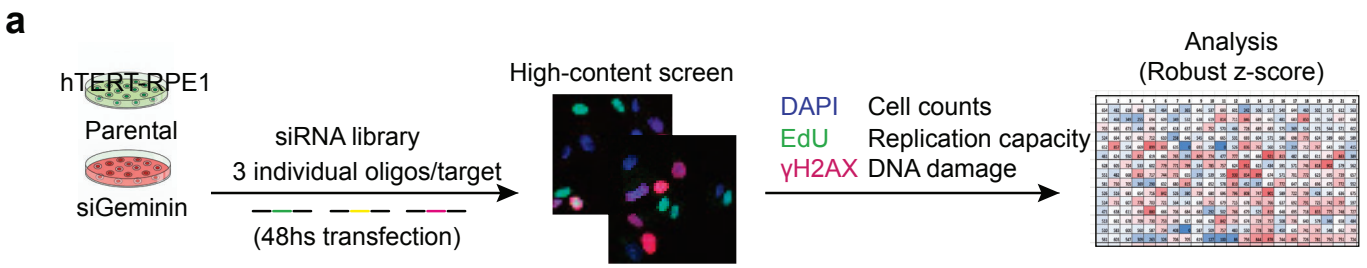

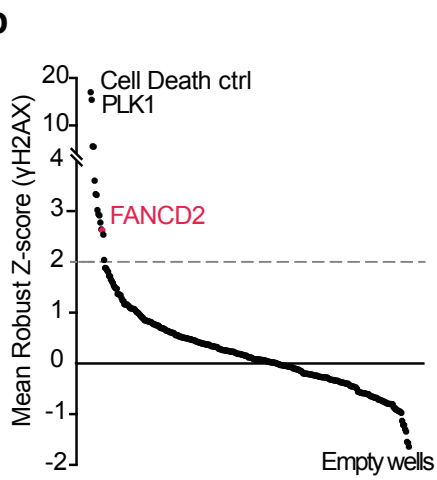

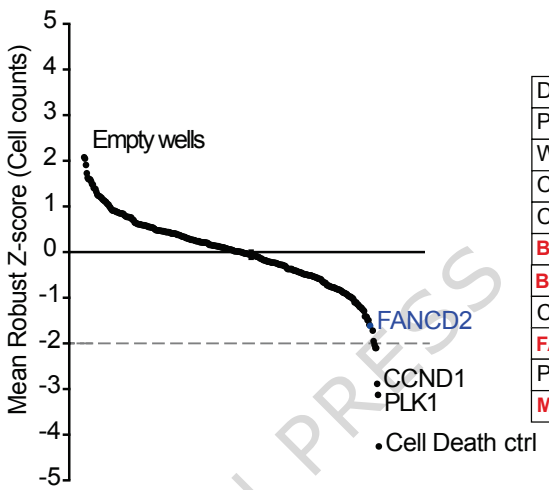

	Mean z-score (γH2AX)		Mean z-score (Cell counts)	
	siGMNN	siCtrl	siGMNN	siCtrl
Death ctrl	19.00	14.89	-4.34	-4.84
PLK1	15.41	12.02	-2.99	-3.29
WEE1	5.62	6.47	-0.01	-0.07
CHK1	3.60	6.36	-0.63	-1.14
CDC20	3.34	7.67	-0.58	-1.65
BRWD3	**3.02**	**-0.32**	-1.35	-0.82
BCL2L2	**2.92**	**0.77**	-1.42	-1.24
CDT2	2.78	5.51	-1.80	-3.34
FANCD2	**2.64**	**0.80**	-1.44	-1.22
PARP1	2.62	1.98	-0.66	-0.73
MDM4	**2.03**	**0.65**	-1.10	-2.09

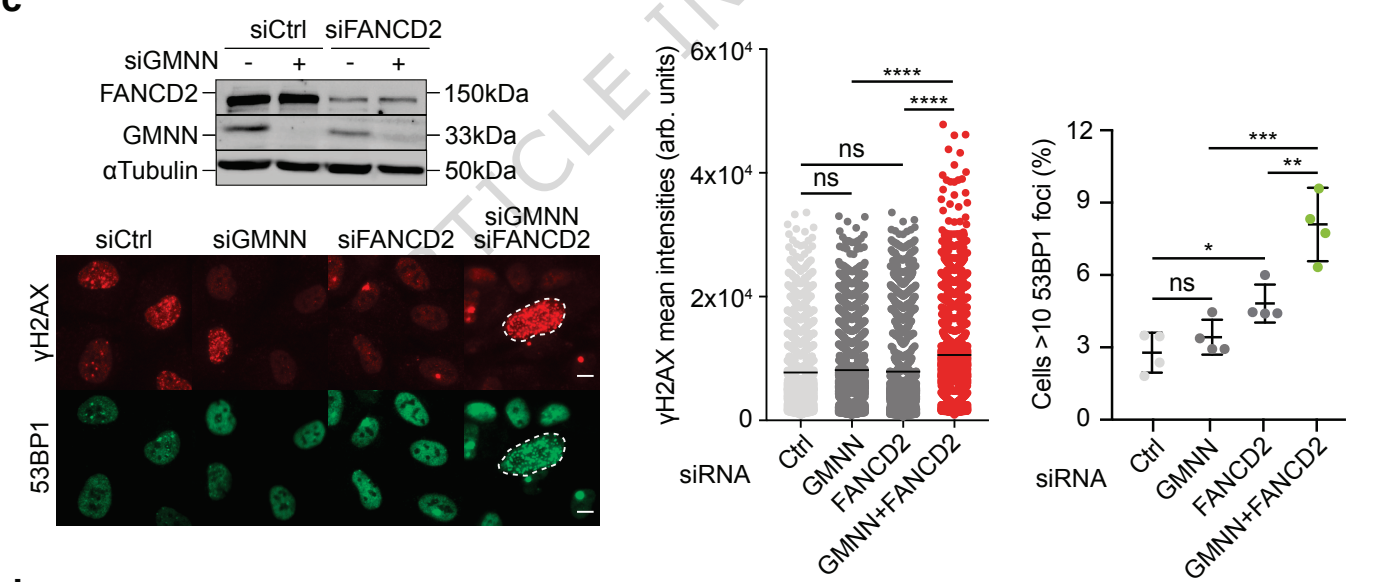

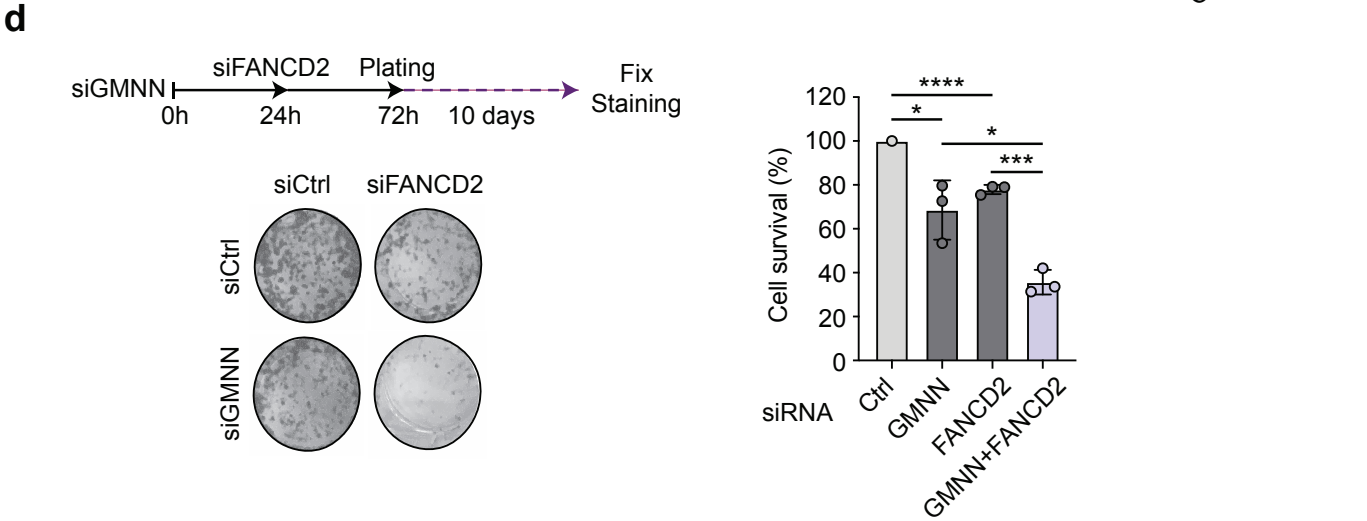

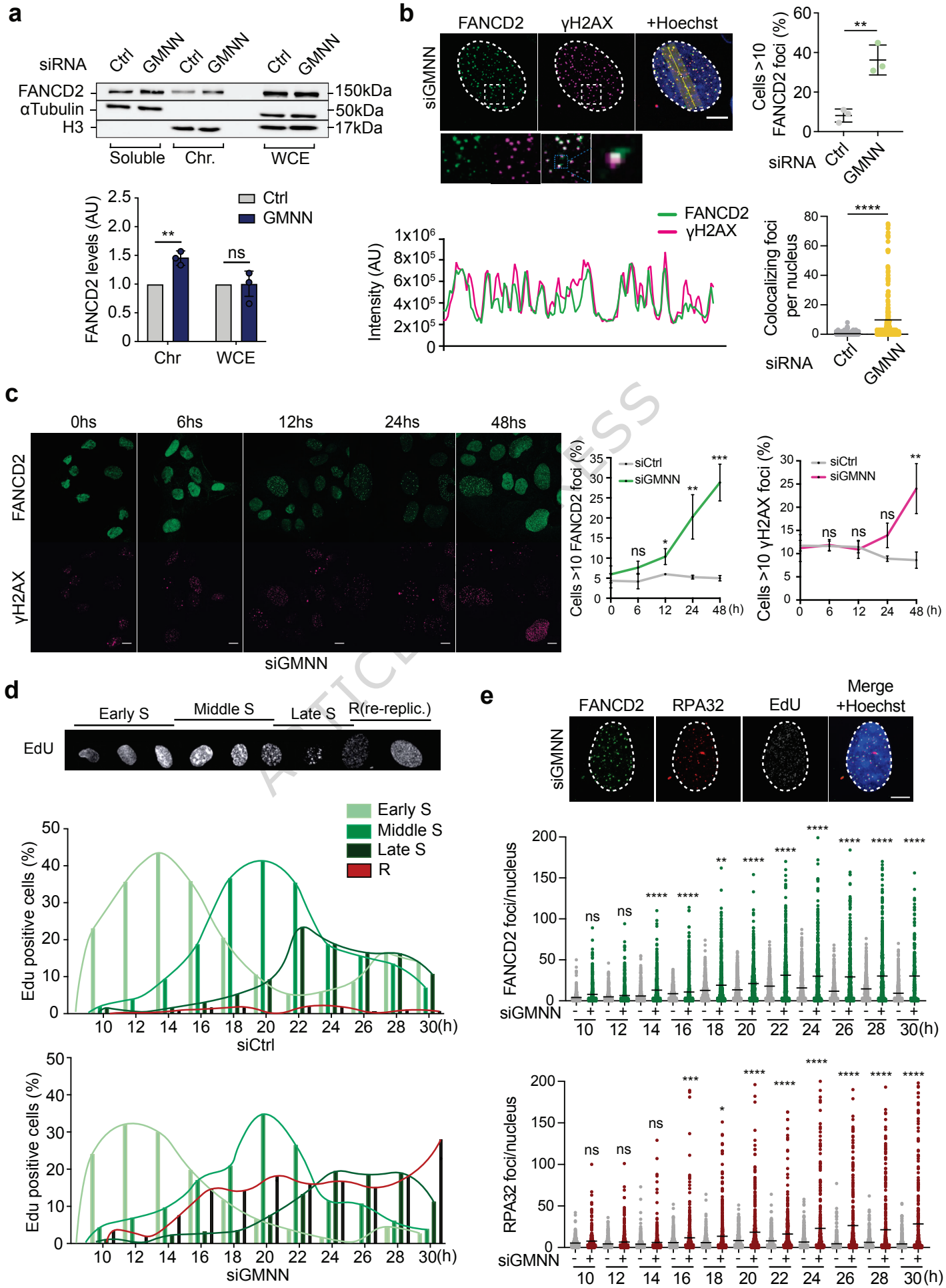
a
siRNA
Ctrl
GMNN
Ctrl
GMNN
Ctrl
GMNN
FANCD2
αTubulin
H3
150kDa
50kDa
17kDa
Soluble
Chr.
WCE
FANCD2 levels (AU)
Ctrl
GMNN
**
ns
Chr
WCE
b
FANCD2
γH2AX
+Hoechst
siGMNN
Cells >10 FANCD2 foci (%)
**
siRNA
Ctrl
GMNN
Intensity (AU)
FANCD2
γH2AX
Colocalizing foci per nucleus
****
siRNA
Ctrl
GMNN
c
0hs
6hs
12hs
24hs
48hs
FANCD2
γH2AX
siGMNN
Cells >10 FANCD2 foci (%)
siCtrl
siGMNN
Cells >10 γH2AX foci (%)
siCtrl
siGMNN
(h)
d
Early S
Middle S
Late S
R(re-replic.)
EdU
Early S
Middle S
Late S
R
Edu positive cells (%)
siCtrl
siGMNN
(h)
e
FANCD2
RPA32
EdU
Merge
+Hoechst
siGMNN
FANCD2 foci/nucleus
siGMNN
RPA32 foci/nucleus
siGMNN
(h)

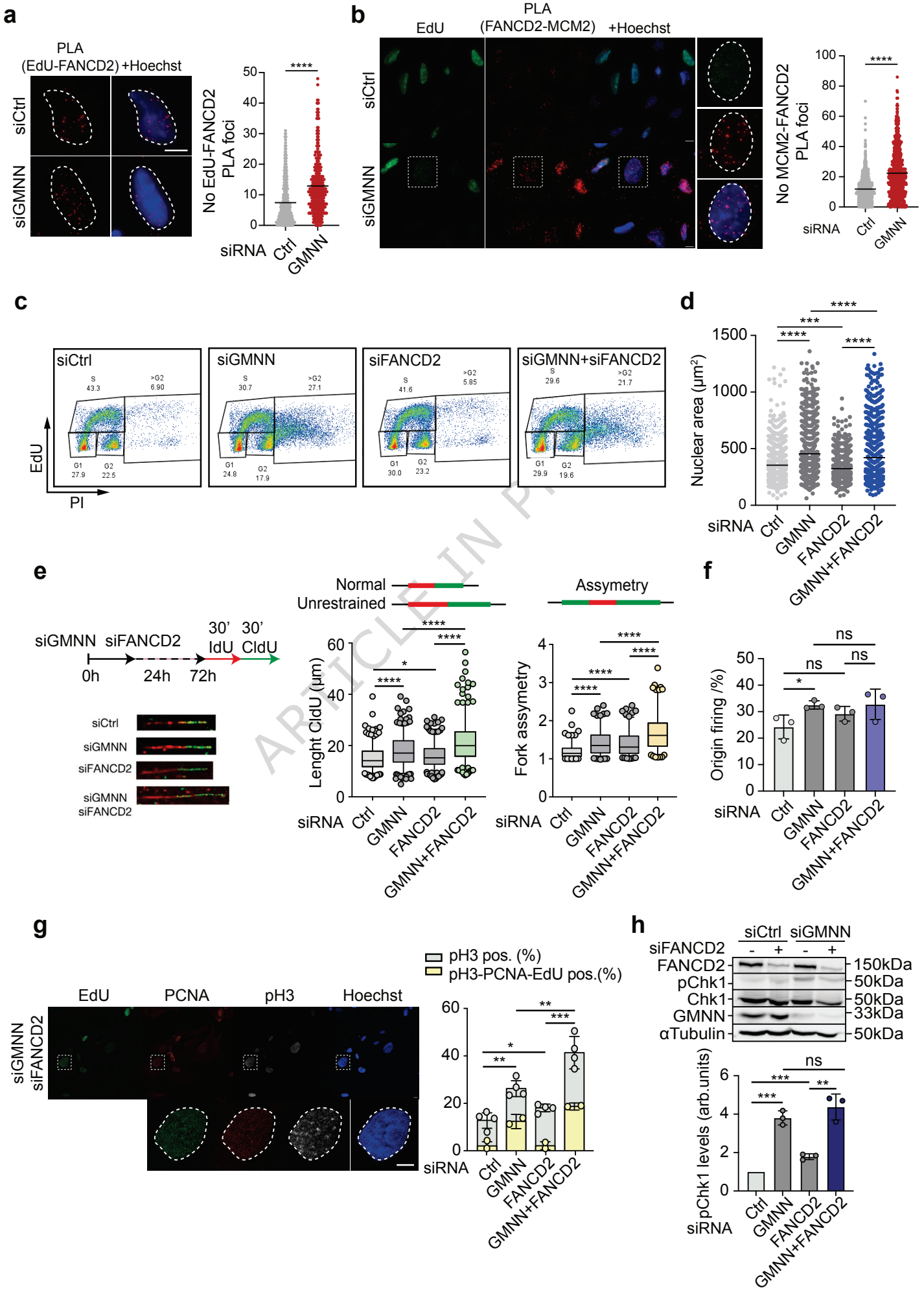
a
PLA
(EdU-FANCD2) +Hoechst
siCtrl
siGMNN
No EdU-FANCD2
PLA foci
siRNA
Ctrl
GMNN
b
EdU
PLA
(FANCD2-MCM2)
+Hoechst
siCtrl
siGMNN
No MCM2-FANCD2
PLA foci
siRNA
Ctrl
GMNN
c
siCtrl
siGMNN
siFANCD2
siGMNN+siFANCD2
EdU
PI
d
Nuclear area (µm²)
siRNA
Ctrl
GMNN
FANCD2
GMNN+FANCD2
e
siGMNN
siFANCD2
30' IdU
30' CldU
0h
24h
72h
siCtrl
siGMNN
siFANCD2
siGMNN
siFANCD2
Normal
Unrestrained
Assymetry
Lenght CldU (µm)
Fork assymetry
siRNA
Ctrl
GMNN
FANCD2
GMNN+FANCD2
f
Origin firing /%
ns
siRNA
Ctrl
GMNN
FANCD2
GMNN+FANCD2
g
EdU
PCNA
pH3
Hoechst
siGMNN
siFANCD2
pH3 pos. (%)
pH3-PCNA-EdU pos.(%)
siRNA
Ctrl
GMNN
FANCD2
GMNN+FANCD2
h
siCtrl
siGMNN
siFANCD2
FANCD2
pChk1
Chk1
GMNN
αTubulin
150kDa
50kDa
50kDa
33kDa
50kDa
pChk1 levels (arb.units)
ns
siRNA
Ctrl
GMNN
FANCD2
GMNN+FANCD2

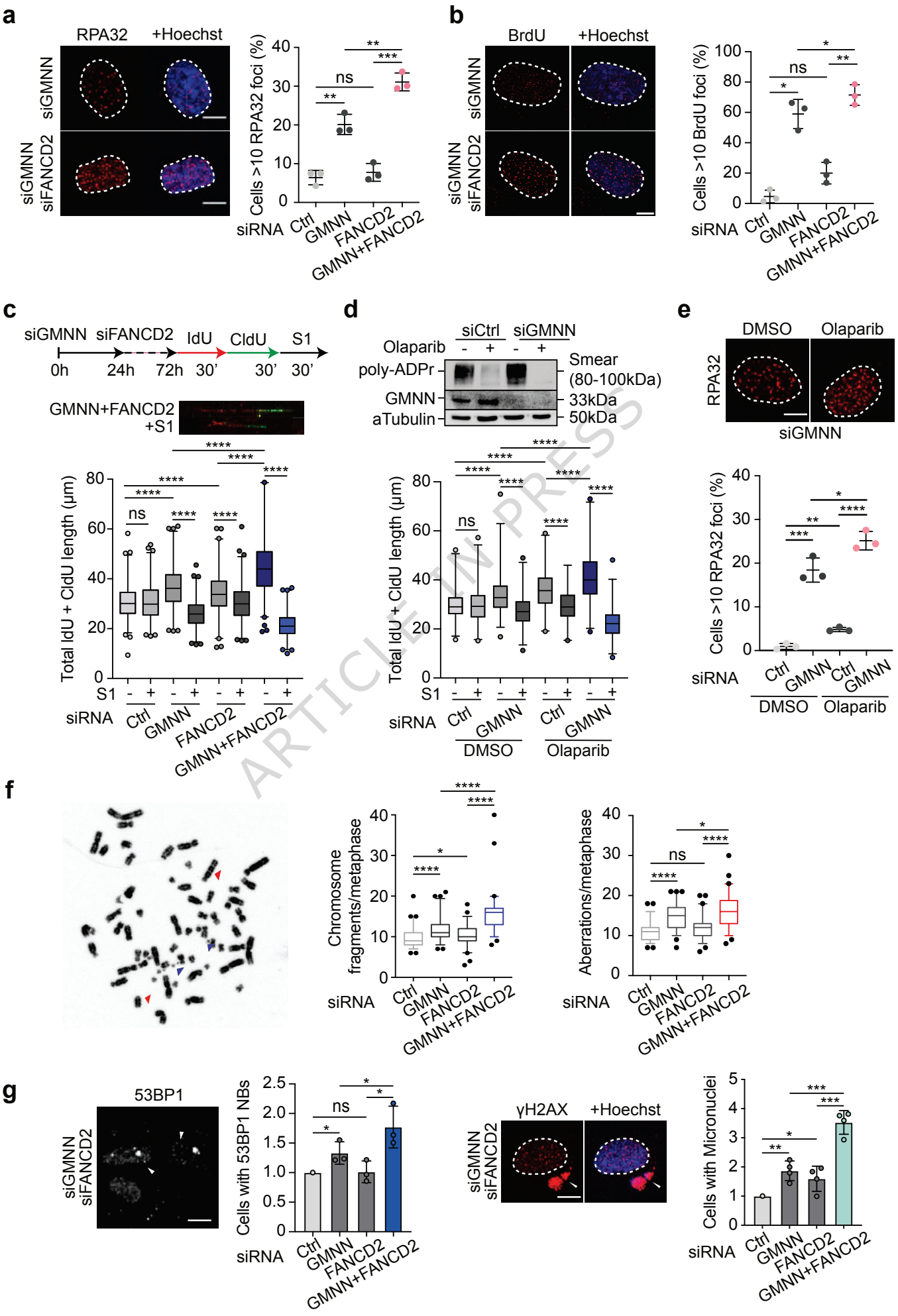
a
RPA32
+Hoechst
siGMNN
siGMNN siFANCD2
Cells >10 RPA32 foci (%)
siRNA Ctrl GMNN FANCD2 GMNN+FANCD2
b
BrdU
+Hoechst
siGMNN
siGMNN siFANCD2
Cells >10 BrdU foci (%)
siRNA Ctrl GMNN FANCD2 GMNN+FANCD2
c
siGMNN siFANCD2 IdU CldU S1
0h 24h 72h 30' 30' 30'
GMNN+FANCD2 +S1
Total IdU + CldU length (μm)
S1
siRNA Ctrl GMNN FANCD2 GMNN+FANCD2
d
siCtrl siGMNN
Olaparib
poly-ADPr
GMNN
aTubulin
Smear (80-100kDa)
33kDa
50kDa
Total IdU + CldU length (μm)
siRNA Ctrl GMNN Ctrl GMNN
DMSO Olaparib
e
DMSO Olaparib
RPA32
siGMNN
Cells >10 RPA32 foci (%)
siRNA Ctrl GMNN Ctrl GMNN
DMSO Olaparib
f
Chromosome fragments/metaphase
siRNA Ctrl GMNN FANCD2 GMNN+FANCD2
Aberrations/metaphase
siRNA Ctrl GMNN FANCD2 GMNN+FANCD2
g
53BP1
siGMNN siFANCD2
Cells with 53BP1 NBs
siRNA Ctrl GMNN FANCD2 GMNN+FANCD2
γH2AX
+Hoechst
siGMNN siFANCD2
Cells with Micronuclei
siRNA Ctrl GMNN FANCD2 GMNN+FANCD2

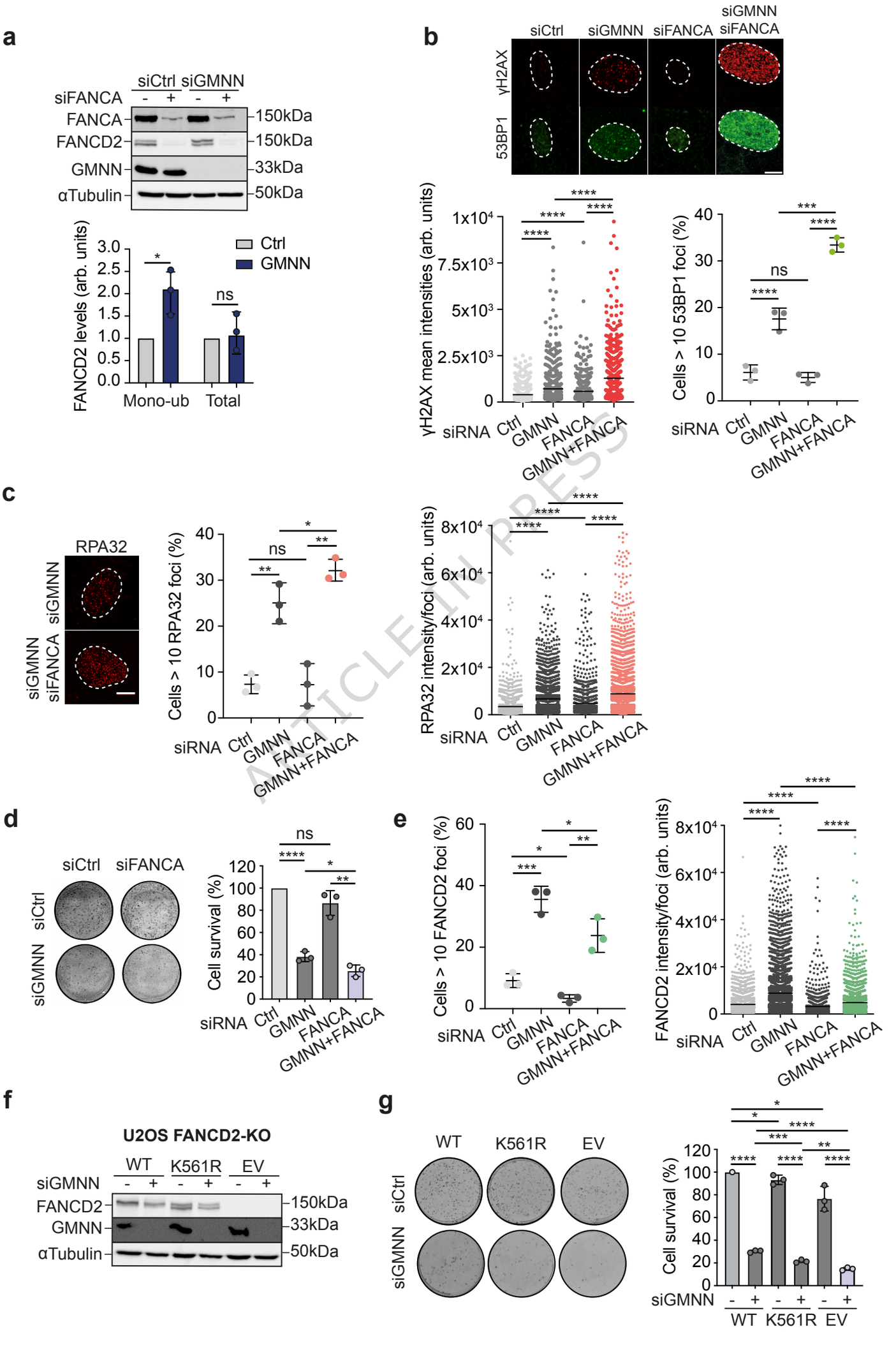

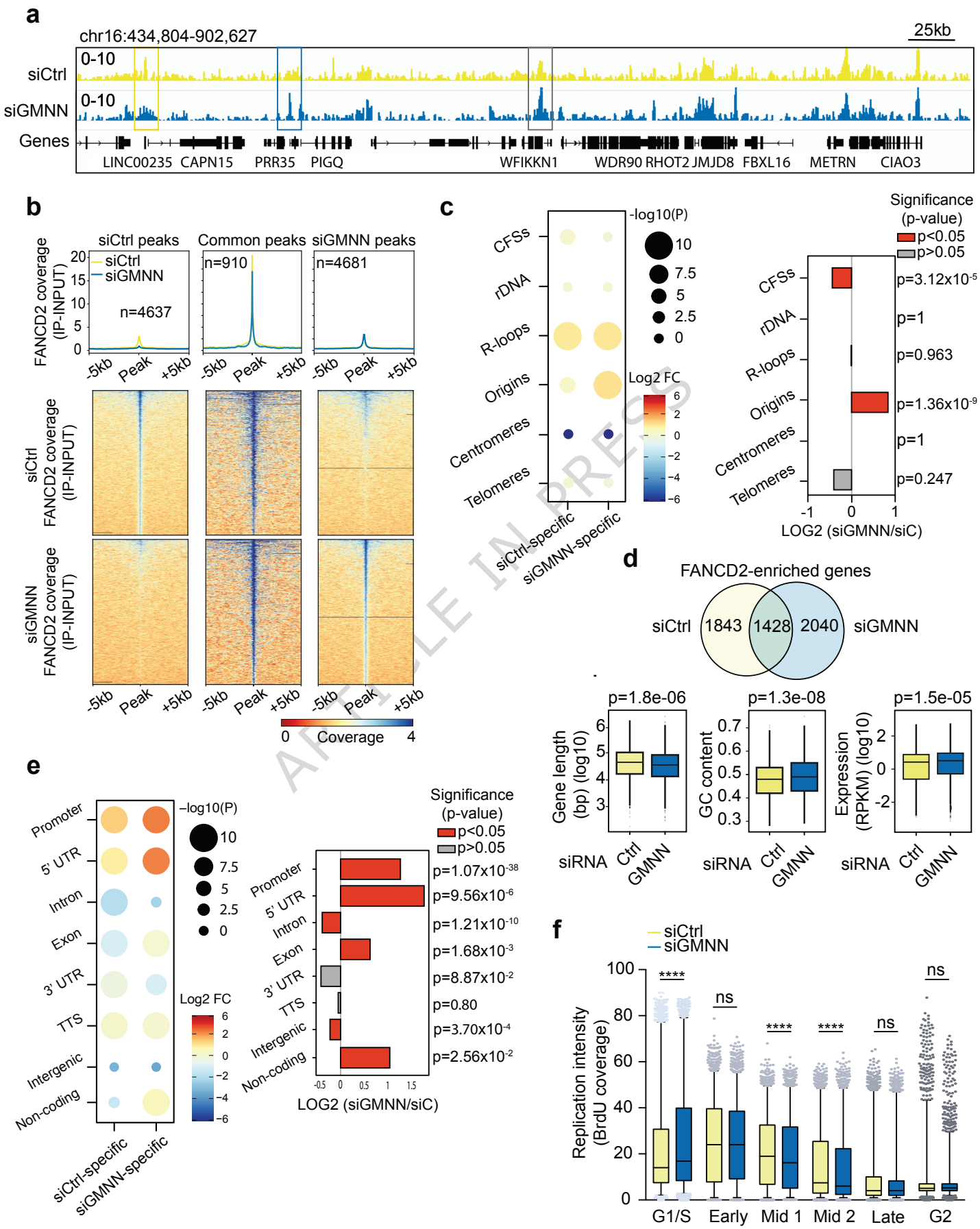
a
chr16:434,804-902,627
25kb
siCtrl
siGMNN
0-10
Genes
LINC00235 CAPN15 PRR35 PIGQ WFIKKN1 WDR90 RHOT2 JMJD8 FBXL16 METRN CIAO3
b
siCtrl peaks
Common peaks
siGMNN peaks
n=4637
n=910
n=4681
FANCD2 coverage (IP-INPUT)
-5kb Peak +5kb
Coverage
c
-log10(P)
Log2 FC
CFSs
rDNA
R-loops
Origins
Centromeres
Telomeres
siCtrl-specific
siGMNN-specific
Significance (p-value)
p<0.05
p>0.05
p=3.12x10-5
p=1
p=0.963
p=1.36x10-9
p=1
p=0.247
LOG2 (siGMNN/siC)
d
FANCD2-enriched genes
siCtrl 1843 1428 2040 siGMNN
p=1.8e-06
p=1.3e-08
p=1.5e-05
Gene length (bp) (log10)
GC content
Expression (RPKM) (log10)
siRNA Ctrl GMNN
e
Promoter
5' UTR
Intron
Exon
3' UTR
TTS
Intergenic
Non-coding
p=1.07x10-38
p=9.56x10-6
p=1.21x10-10
p=1.68x10-3
p=8.87x10-2
p=0.80
p=3.70x10-4
p=2.56x10-2
f
siCtrl
siGMNN
Replication intensity (BrdU coverage)
****
ns
G1/S Early Mid 1 Mid 2 Late G2